SOUND-DRIVEN MODULATION OF TACTILE RESPONSES IN THE MOUSE SOMATOSENSORY CORTEX

by

Manning Zhang

A thesis submitted to Johns Hopkins University in conformity with the requirements for the degree of Master of Science and Engineering

Baltimore, Maryland

May, 2017

ABSTRACT

Central to cognition is the ability to resolve and interpret information emerging from disparate physical senses. This process, termed multisensory integration, is thought to be implemented through neuronal computations; however, where and how exactly such processing occurs in the brain remains to be fully elucidated. To this end, the primary and secondary cortices have been traditionally studied according to their dominant sensory modality. Even so, recent studies hint at the possibility of multimodal interactions in these brain regions. Here we systematically probe multimodal integration of sound and touch representations in the rodent somatosensory cortex using two-photon Ca^{2+} imaging. We find that pairing sound with tactile stimuli modulates the activity of a significant population of tactile responsive neurons in both primary and secondary somatosensory cortices. While the polarity of this modulation can be either inhibition or facilitation, inhibition dominates for a majority of neurons. Moreover, the strength of this inhibition depends upon the frequency of tactile stimulation, with lower frequency responses more severely attenuated. Intriguingly, we also found a subpopulation of neurons in the secondary somatosensory cortex that are sound-selective with no apparent responses to tactile stimuli. The activity of these neurons is inhibited by high-frequency tactile stimuli reflecting symmetric multimodal operations. Overall, these results suggest that multisensory integration pervades neuronal processing in both primary and secondary cortices. Our findings comment upon the exquisite nature of multimodal interactions in the brain and further sets the stage for in-depth mechanistic studies to dissect microcircuits that underlie these complex computations.

Thesis readers: Manu Ben-Johny, Ph.D.; Daniel H. O'Connor, Ph.D.; Kechen Zhang, Ph.D.

ACKNOWLEDGEMENTS

Having been half an earth away from home for two years, I miss my family so much. Without their support and understanding, I would have no way of completing my studies here. First, I want to thank my grandparents. Because my mom and dad worked away from home when I was younger, I spent most of my childhood with my grandparents. They raised me and shaped my personality the most. My grandfather is a romantic man full of love towards the beauty of life and nature. He is the kind of person that, even with something as simple as taking a shower, he would choose to take the shower in the greenhouse so that he could appreciate his flowers and plants. We spent a lot of time just sitting and staring at plants together. He also passed his enthusiasm for cooking onto me, which helped me survive through the past two years. My grandmother dedicates her every effort to give her children a better life. She fed me a lot since I was a baby. This trained me to have a strong stomach to digest everything I want without worrying about eating too much.

Next, I want to thank my parents. I am their only child. In the past two years, when other families get together for holidays or festivals, I cannot be with them. Although they have never complained about this to me, I know my absence made them feel lonely many times. For me, my mom is more like my closest friend. She kept me company when I started to live with them. We fought with each other for the last cookie and sat together waiting for the sun to rise into the sky. She mimicked what is death for me and let me try my first surgery on her wounded finger. She is the most optimistic woman I have ever met. And her deep sympathy for many things helped me retain my humanity even after diving into the deep dark ocean of science. She introduced me to music so that I can appreciate and express emotions without saying a word. Her hobby of reading led me to become a big fan of history and archaeology. She educated me to become a happy person

that can appreciate the colorfulness of life. I hope I will never let her down. My father is an interesting person who always supported me fully. No matter if I wanted to steal some candy from my mom or decided to cut holes in her favorite sweater as a declaration of "war", he always told me, "We are a team". At many moments when I feel uncertain about my future, his support gives me bravery to choose what I really want. Although I never believed the rocks he randomly kidnapped to bring home during his walks contain real jade, his passion made me realize that we live individually in a lonely planet. You need to be the one who really likes what you do.

During my time at Hopkins, many people have helped me complete my studies and become a better researcher. Initially, I came to Hopkins through a summer research program. Dr. Kechen Zhang was the first mentor I met here. He not only gave me the chance to start a summer project in his lab, but he also helped me a lot with my applications to graduate schools. Dr. Joe Monaco is a postdoc fellow in Dr. Zhang's lab who helped me immensely with my summer project and taught me how to use Python. Dr. Raimond Winslow gave lovely lectures and challenging midterm questions during the *Models of the Neuron* class. I enjoyed it very much.

Dr. Daniel O'Connor is one of my mentors after Dr. David Yue passed away. He is always very helpful and offered a lot of advice and equipment to help us undertake this project. And his advice on graduate school made me suddenly realize what is really important about graduate school, that it is about science and curiosity and not just about myself. Dr. Sam Kwon is a postdoc fellow in Dr. O'Connor's lab. He gave us many suggestions on our project and helped us with intrinsic imaging experiments that were needed to validate our own imaging results.

Zixuan Lin, a graduate student of BME, is my close friend since senior year. She is always very good at handling coursework. I really enjoyed our short talks on the shuttle heading back from Homewood to the medical campus after class. Xiaoxuan Zhang, Qiang Li, Haiyuan Li,

Cunfang Qi, Shu Huang – they stepped into my life since my first year here. We always have a lot of fun hanging out together.

I feel strong emotional attachment with the Calcium Signals Lab (CSL). People here have given me more help than I could imagine. Wanjun Yang, the technician of CSL, is my little mom in the lab. She took care of me a lot. Because of her presence. I have had a chance to speak Chinese and complain about my courses and experiments. I really enjoyed talking with her about my daily life and sharing some memories about China. Jacqueline Niu is a BME graduate student, who is also my funny roommate. She brought so much fun to my life. We went out for food, cooked dinners, talked about life and religion, and watched hilarious dramas featuring her favorite actor. She always cracked jokes for me and I always try to insult her as payback. We laughed together a lot about so many random things. She is my best audience for the food I made. And I will always miss her "refreshing uselessness" after I move on. Po Wei Kang, a former master student in CSL, is our lunch time clock when he was here. I was so impressed by his calmness. One time a mouse jumped from my hand and ran on the bench. I was screaming in my heart and I did not know how to deal with it. Then I saw Billy pick up the mouse tail and put it into my cage with a poker face. Ivy Dick, a former postdoc fellow here, has been very helpful on many occasions. She stepped up and helped us through the hard times after Dr. Yue passed away. I will always be grateful for her help. Rahul Banerjee, a postdoc fellow in our lab, always has a warm smile on his face. Lingjie Sang, a former graduate student, who also happens to be from my hometown, shared many of her precious experiences with me about living here as a foreigner. Jiangyu Li, a former master student, has the most impressive skills with eating blue crabs. She gave me many suggestions about classes when she was here. During my time in CSL, there are also some other good people that I would like to thank for their help here: Worawan Limpitikul and Ho Namkumg.

John Issa, the “rule breaker” in CSL, is my most direct mentor during these two years after Dr. Yue passed away. I feel ashamed to admit the fact that his brain process information 1.5 times faster than me. He trained me on everything from the beginning. And I was always impressed by his systematic thinking, curiosity, and creativity when we designed a new experiment or built a new set-up. He is always very generous with spending his time discussing our project or explaining some basic knowledge about calcium imaging to me. Other than the project, he is also a great mentor who is really willing to share advice about life with me. Influenced by him, I learned to study hard for every course and tried to become a better student. His attitude towards science inspired me the most. I will never forget the scene when he was standing by the trash box in 724, smiling and said, “Doing science is not like doing politics. No matter what we find, it will stay forever. And forever is a long time”. Moreover, I really appreciate that he would laugh at my most crappy jokes and tried without hesitation every time when I brought food to the lab. I will always look up to him and try to become a scientist, a mentor, a person like him.

Manu Ben-Johny, my other mentor in the CSL, is someone I really respect. He vouched for my study in this program two years ago. And he is very patient, as well as willing to spend his time teaching me how to think linearly, organize a better story, and make figures more beautiful. He always cares about my growth and tries to help me. Much of his advice is very sharp and valuable, which I take into my heart. He is a very good scientist and always has many good ideas. I will carry his enthusiasm towards science as I try to find my own path in graduate school.

Dr. Gordon Tomaselli helped our lab a lot after Dr. Yue passed away. He provided many suggestions and support for this project and my applications. Although he is a cardiologist, he was always the most eager to participate and learn about my journal clubs on neuroscience topics and progress of my project. I will always be grateful for his kindness.

Last but not least, I want to thank Dr. David Yue for bringing me into the CSL family. Without him, I would have had no chance to study here, get so much help from all the good people mentioned above, and carry out this project. In this regard, he magically changed my life. Although Dr. Yue passed away shortly after I joined the lab, I learned about how good of a scientist, a mentor, and a friend he is from how he affected the people surrounding him. Studying in the CSL for the past two years is not only a process to train myself to do science, but also gradually to pick up part of his enthusiasm, humbleness, and optimism when pursuing science. I will carry his spirit and try to grow up into a good researcher whom both he and I would be proud of.

TABLE OF CONTENTS

LIST OF FIGURES

CHAPTER 1

Introduction

At each moment of our life, we receive concurrent inputs from each of our many senses. To form a holistic percept, we must seamlessly integrate these sensory inputs to ultimately shape our experiences and to inform our everyday decisions. For example, when playing music on a piano, we may press the keys more gently or heavily depending on the desired volume and the flow of music. To successfully execute this seemingly simple task, our brains must integrate auditory, visual, tactile, and proprioceptive cues. In fact, most human behaviors rely on the ability to discern and to bind multisensory input, with unisensory signaling dominant only under special circumstances.

In humans, psychophysical studies have demonstrated multimodal integration in diverse settings – for example, between auditory and visual cues ("McGurk effect") (McGurk and MacDonald, 1976), tactile and visual cues (Lunghi et al., 2014), and tactile and auditory cues (Lederman et al., 2002). In particular, interactions between the somatosensory and auditory system have been long-recognized (Jousmäki and Hari, 1998). Synchronous auditory feedback can powerfully modify perceived tactile stimuli, an effect known as the "parchment-skin illusion" (Jousmäki and Hari, 1998). In this illusion, the perceived roughness or moisture of palmar skin decreases when subjects simultaneously listen to high-frequency sounds. Multisensory integration is thus essential to formulate a coherent understanding of the external environment, yet its neurobiological basis – i.e. where and how sensory binding and downstream processing occurs – remains to be fully elucidated.

Where does multisensory integration occur? Some multisensory integration occurs in subcortical areas. The dorsal cochlear nucleus (DCN), an auditory processing station located in the brainstem, receives somatosensory inputs from muscle receptors associated with the pinna. This information is then used to coordinate pinna orientation during sound localization (Kanold and Young, 2001). The superior colliculus coordinates inputs from numerous sensory modalities, including vision, audition, and touch (Wallace et al., 1993), to eventually direct head and eye movements towards the an external stimulus (Frens et al., 1995; Stein and Alex, 1993; Stein et al., 1989). Responses to sound in the inferior colliculus, a midbrain structure involved in sound localization, are modulated by information about head and eye position provided by the visual system (Groh et al., 2001).

Multisensory information from these subcortical areas may be carried by feedforward inputs to primary cortical regions (Foxe and Schroeder, 2005; Giard and Peronnet, 1999; Stein and Stanford, 2008); however, primary cortical regions are traditionally thought to be predominantly involved in unisensory processing (Jones and Powell, 1970). Rather, some multimodal integration has been observed in cortical regions adjacent to the primary sensory cortices of primates. Multielectrode array recordings of the primary somatosensory and auditory cortices revealed that neurons within these regions are largely devoted to processing their principal sensory stimuli (Lemus et al., 2010). More specifically, neurons in the primary somatosensory cortex robustly encoded tactile stimuli and their responses were largely indiscriminate to sound stimuli. Similarly, while neurons in the primary auditory cortex were highly responsive to acoustic stimuli, these neurons failed to encode tactile information. On the other hand, a few neurons in the secondary somatosensory cortex appeared to encode information pertaining to both tactile and auditory stimuli. These findings led the authors to suggest that the primary cortices are largely devoted to

unimodal processing while multimodal processing is likely initiated in secondary cortical regions (Lemus et al., 2010). However, other primate studies have argued that neurons in primary somatosensory cortex (Broadmann area 3a, 3b, 1, 2) may participate in the integration of sound information with other sensory information while performing behavioral tasks (Zhou and Fuster, 2004). Likewise, fMRI studies in humans and anesthetized macaques showed integration of tactile and auditory stimuli in cortical areas near to the primary auditory cortex (Brosch et al., 2005; Foxe et al., 2002; Kayser et al., 2005). Moreover, single-unit recordings in macaques also demonstrated that neurons within an area adjacent to the primary auditory cortex responded to cutaneous stimuli (Fu et al., 2003). In all, the question of whether neurons within primary sensory cortices process and encode multisensory information remains to be fully examined.

Higher-order cortices that receive inputs from various primary cortical regions are thought to play a key role in multisensory integration in primates. For example, a large fraction of neurons in the ventral intraparietal area have been shown to be bimodal, responding robustly to either visual or tactile stimuli (Duhamel et al., 1998). These neurons are thought to be critical for construction of a head-centered representation of the nearby environment. In like manner, neurons within specific sub-regions of the posterior parietal cortex of primates combine visual, somatosensory, auditory, and vestibular signals to formulate a spatial reference frame for a given stimuli with respect to the observer and within an environment (Andersen, 1997). The caudal superior temporal sulcus has been shown to have multimodal neurons responsive to visual, auditory, and somatosensory inputs (Hikosaka et al., 1988). The premotor cortex, similarly, contains neurons that respond to both visual and somatosensory stimuli (Graziano et al., 1994). In this manner, multiple higher order cortical regions contain multimodal neurons, all helping the brain to construct a complete representation of the surrounding environment.

Recent studies of rodents have also identified multimodal integration in numerous cortical regions. For example, two-photon Ca^{2+} imaging using fluorescent dyes revealed multisensory interactions between visual and tactile inputs in neurons in an area interposed between primary visual and somatosensory cortices (Olcese et al., 2013; Zhuang et al., 2017). *In vivo* whole-cell recordings in layer 2/3 pyramidal neurons in primary sensory cortices have revealed widespread hyperpolarization in response to stimuli from non-preferred sensory modalities. And sound-driven synaptic inhibition was observed in primary visual cortex (Iurilli et al., 2012). The relative ease of genetic manipulation of mice furnishes a convenient platform to dissect fundamental circuit-level mechanisms underlying multimodal sensory processing, an exciting frontier.

What are functional features of multimodal integration? While many studies have found evidence for multimodal interactions at different stages of sensory processing in the brain, it is unclear how much is due to gain modulation and how much involves a genuine computational component. For example, attentional state is known to change the gain of cortical responses (Moran and Desimone, 1985; Roelfsema et al., 1998; Treue and Trujillo, 1999), and thus multimodal interactions may be secondary to attentional changes in the presence of conflicting inputs from two sensory modalities. However, in human studies, there is some evidence for more complex circuit computations that rely on specific temporal features such as frequency, a key aspect of both auditory and somatosensory information (Yau et al., 2009, 2010). Here, subjects were asked to discriminate the frequency of either a tactile or auditory stimulus. When adding a distractor that was presented before the attended stimulus, it was found that the effect on frequency discrimination was the same regardless of whether the distractor was tactile or auditory in nature. Furthermore, there was a disconnect between the effects of frequency and intensity discrimination. Bias in intensity discrimination only happened when the distractor was tactile. The relative timing

between auditory and somatosensory inputs was a factor for intensity discrimination but not for frequency discrimination. These lines of evidence indicate that the interaction of frequency and intensity between these two sensory modalities may be mediated by divergent neural mechanisms (Yau et al., 2009, 2010). Mathematical modeling of this interaction showed that the auditory distractor shifted the highest-response tactile frequency, resulting in a change in tactile discrimination performance (Crommett et al., 2017).

Why is frequency important for somatosensory sensation? Human are capable of sensing mechanical vibrations up to 1 kHz through skin surface receptors (Crommett et al., 2017). This ability is believed to be crucial for texture sensation (Manfredi et al., 2014) and sensing the external world through hand tools (Johnson, 2001). For rodents, vibration is sensed through mechanical receptors located in whisker follicles, and this information is sent through the trigeminal nerve to the brainstem and thalamus(Diamond et al., 2008). In thalamus, the ventral posteromedial nucleus (VPM) sends its outputs primarily to the primary somatosensory cortex, while the posterior nucleus (POm) sends its outputs to both primary and secondary somatosensory cortices. Secondary somatosensory cortex mainly receives thalamic input from the POm (Bosman et al., 2011). POm and VPM cells have different response properties. Cells in POm show earlier adaptation to whisker stimulus frequency than VPM cells (Diamond et al., 1992), a difference that may be reflected in the different response properties of primary and secondary somatosensory neurons. In texture discrimination tasks, rodents have the ability to distinguish smooth surface textures from rough textures using their whiskers. This process is conducted within hundreds of milliseconds and is typically characterized by a dominant 8 Hz whisker sweep behavior (Carvell and Simons, 1990). Finally, recordings in rodent primary somatosensory cortex have shown a direct link between neuronal firing rate and texture judgement (von Heimendahl et al., 2007). Thus, it appears that

frequency is a very important aspect of tactile information that is used for discriminating surface texture and the different thalamocortical tracts may serve distinct roles related to frequency discrimination.

Previous studies have shown that multimodal integration between auditory and somatosensory inputs can occur at different stages of the sensory processing pathway; however, little is known in a large imaging scale with single neuron level accuracy. Meanwhile, finer control of tactile and auditory stimuli is needed to reveal more information about the computation of multimodal integration. Here we designed our tactile and sound stimuli using frequency as a major component and performed large-scale Ca^{2+} imaging with two-photon microscopy in 5 mm chronic windows, chosen such that they can span both primary and secondary somatosensory cortices as well as much of the auditory cortex. Our approach uncovered frequency-dependent suppression of tactile responses in mouse primary and secondary somatosensory cortices. Moreover, these effects were dependent on the frequency tuning of touch-responsive neurons.

CHAPTER 2

Methods

Animal Surgery and General Procedures

All animal procedures were approved by the Johns Hopkins Institutional Animal Care and Use Committee. Imaging experiments utilized transgenic mice expressing the genetically encoded Ca^{2+} indicator GCaMP6s (Chen et al., 2013) under a pan-neuronal promoter. Most experiments used GP4.12 Thy1-GCaMP6s mice (JAX No. 025776) (Dana et al., 2014). A small subset of tetO-GCaMP6s mice (JAX No. 024742) were also used for imaging (Wekselblatt et al., 2016). Finally, lox-GCaMP6s mice (JAX No. 024106) (Madisen et al., 2015) were crossed with Syn1-Cre mice (JAX No. 003966) (Zhu et al., 2001), resulting in lox-GCaMP6s-Syn1-Cre mice. In total, 12 males and 5 females were used. Among them, 14 were GP4.12 Thy1-GCaMP6s mice, 2 were tetO-GCaMP6s mice, and 1 was a lox-GCaMP6s-Syn1-Cre mouse.

For surgery to implant headposts and chronic imaging windows, anesthesia was provided by 1-1.5% isoflurane in 0.5 L/min O_2. Body temperature was maintained at 37^{o}C with a heating pad and monitored through a rectal probe. Carprofen (5 mg/kg, i.m.) and dexamethasone (5 mg/kg, i.m.) were injected to limit inflammation. Lidocaine (20 mg/ml) was injected locally at the incision site as a pain blocker. Normal saline (0.50 ml, i.p.) was injected at the end of the surgery to avoid dehydration. Skin covering the left hemisphere of the mouse was retracted to expose skull overlying auditory and somatosensory cortices. Skull was afixed to a custom headpost using a UV-cured primer (Kerr OptiBond) and dental cement (Heraeus Charisma A1). A 4-5ø mm craniotomy spanning both auditory and somatosensory cortices was performed. After removing the skull, the craniotomy was filled with a transparent silicone gel (3-4680, Dow Corning, Midland, MI)

(Jackson and Muthuswamy, 2008) to help maintain the stability and clarity of the chronic window. Next a 4 or 5 ø mm (No. 0 or 1) cover glass was secured with dental cement above the window. After surgery, mice were periodically given carprofen (5 mg/kg, i.m.) and dexamethasone (5 mg/kg, i.m.) for inflammation and buprenorphine (0.1 to 0.5 mg/kg, s.c.) for pain. Mice were given 10-14 days to recover before imaging sessions were started.

Experimental Setup

During imaging sessions, all mice were awake and head-rotated approximately 45^{o} to make the imaging plane perpendicular to the microscope objective. Mice were first adapted to running on a custom-built treadmill while head-fixed for 1-2 session of 20 to 40 minutes each. Once habituated, imaging sessions began. Mice were able to tolerate head fixation for up to 2 or 3 hours. Running speed was recorded with an optical encoder (E5-2500-188-IE-S-H-D-B, US Digital). For whisker stimulation, all whiskers of the right whisker pad were trimmed except for the C2 whisker, facilitating isolated stimulation of a single whisker.

Imaging

For widefield imaging, a white light source (LED Engin LZ1-10CW00) was used for illumination. Illumination light and fluorescence signals were filtered through a GFP filter cube (460/50 excitation, 540/50 emission). A 10× 0.25 NA objective (Olympus) and a Photometrics Evolve 512 Delta camera were used to collect the emitted light. The field of view was roughly 2.2 x 2.2 mm^2. The imaging speed was 20 Hz. Illumination power density was 0.25 mW/mm^2 and pixel size was 4.4 x 4.4 $microns^2$. Additionally, a 4× objective was used first to localize both auditory and somatosensory cortices in the window based on functional responses to acoustic and tactile stimuli.

Two-photon Ca^{2+} imaging was performed with an Ultima system (Prairie Technologies) built on an Olympus BX61W1 microscope. A mode-locked laser (Coherent Chameleon XR Ti:Sapphire) tuned to 950 nm was raster scanned at 5 Hz for excitation while emitted GCaMP6s fluorescence was collected through a green filter (525/70 nm). Laser power at the sample was 20-80 mW. Dwell time was set to 2 μs. To increase the imaging speed, resolution along the *y*-axis was reduced by a factor of 4. The final pixel size was 0.9x3.6 μm. A 20× 1.00 NA objective (Olympus) was used to yield a 465x465 μm^2 field of view. Imaging depths were between 150-500 μm, with 94% of imaging fields between 200-350 μm.

Stimuli

Tactile Stimuli

To stimulate the target whisker on the right side of the whisker pad, we used a piezoelectric bending actuator (Q220-A4-203YB, Piezo systems, Inc., MA) moving in the rostral-caudal direction. We attached a 2 cm sewing needle to the long axis of the piezo and passed the target whisker through the needle eye at a distance of 2 mm from the face. The needle coupled the whisker to the piezo movement. The shape of the needle allowed the whisker some freedom to move in the medial-lateral direction but not in the rostral-caudal direction. To facilitate precision in the positioning of the needle, we attached the piezo to a micro-manipulator (MT-XY Compact Dovetail Linear Stage, Newport Corporation). The piezo itself was driven by a voltage driver (MDT694B, Thorlabs) with a 10 x gain. Thus, the 0-10 V signal delivered by the DAQ card was expanded to a range of 0-100 V used to drive the piezo.

A single tactile stimulus consisted of a 500 ms sinusoidal wave. One tactile trial consisted of a set of sixteen individual stimuli with a 2 s interval between each presentation. The frequency

of each sinusoidal stimulus consisted of a frequency chosen from our range of 2 to 128 Hz, spaced logarithmically and the order randomized (Figure 1A). The amplitude of piezo deflection was 0.6 mm. With the needle ~2 mm away from skin surface, a 2 Hz stimulus was equivalent to an angular velocity of ~70^{o}/sec. Thus, angular velocity of our tactile stimuli is calculated from the frequency as angular velocity = 35^{o}/sec x (frequency), where frequency is given in Hz. In this work, we report the stimulus parameters in frequency.

Monthly calibration of the piezo deflection amplitude and capacitance was essential since the piezo was easily broken. Calibration was done by imaging piezo movement at high speeds with the Photometrics Evolve 512 camera for a given deflection frequency. Maximum deflection displacement was measured and angular velocity was calculated. Once angular velocity dropped by more than 20%, the piezo was replaced.

An important consideration in this work was whether the delivery of tactile stimulation with the piezo generated any audible noise that the mouse could hear. To determine the noise level and whether it is within the hearing range of mice, we performed a noise calibration while controlling the piezo at frequencies ranging from 2 to 256 Hz. Sound was recorded with a probe tube designed by G. Sokolich. The Sokolich probe can detect sound frequency up to 100 kHz. To ensure that we picked up all the possible noise generated by piezo movement, we placed the Sokolich probe directly next to the piezo. We found that, across the mouse hearing range (3-100 kHz), no audible noise was generated as long as the frequency of piezo deflection was kept lower than 140 Hz. Above 140 Hz, though, audible sounds were generated. Thus, all stimuli used in this study were limited to a maximum of 128 Hz. To test the opposite, whether acoustic stimuli could cause any vibration of the piezo, we imaged the piezo at 363 Hz while playing sounds at the

maximum amplitude possible with our speakers. We found no detectable movement of the piezo under imaging.

Auditory Stimuli

The imaging set-up is located in a sound-attenuated room (Acoustical Solutions, AudioSeal ABSC-25) with noisy equipment located outside the room. Noise calibrations showing ambient noise to be outside the mouse hearing range have been previously published (Issa et al., 2014). Sound stimuli were delivered through a free-field speaker (LCY K100, Ying Tai Corporation) located 15 cm away from the right ear. We used sinusoidal amplitude modulated (SAM) tones as sound stimuli. These are defined by two parameters: the carrier frequency, which is typically in the kHz range, and the SAM frequency, which forms the amplitude envelope and is in the range of 2 to 256 Hz. To keep the terminology consistent, we refer to each SAM tone by the carrier frequency first and the SAM frequency second. For example, "100 Hz, 8 Hz SAM tones" refers to a 100 Hz carrier frequency with an 8 Hz SAM envelope, as shown in Figure 1B. To keep a consistent terminology, we used the first number to denote the carrier frequency, and the second number to denote the SAM frequency. For example, in Figure 1B, we showed a schematic waveform of 100 Hz (carrier frequency), 8 Hz (SAM frequency) SAM tones in 500 ms stimulus duration. Our auditory stimuli consisted of sixteen SAM tones with a fixed carrier frequency and a fixed SAM frequency. Their carrier frequency covered the whole hearing of mouse (3-96 KHz). The duration of each stimulus was 500 ms. All the stimuli were delivered in a random order and with a 2 s interval. Stimuli were played at -40 to -20 dB attenuation, corresponding to ~60-80 dB SPL using our speaker.

Combined Stimuli

Combined stimuli consisted of simultaneous presentation of the auditory and tactile stimuli described above. The tactile stimuli were sixteen tactile deflections with different frequencies ranging from 2-128 Hz while a fixed auditory stimulus consisting of a fixed carrier frequency and SAM frequency was added to each of the sixteen tactile stimuli. Each stimulus lasted 500 ms and the tactile and auditory stimuli were coinitiated and coterminated (Figure 1C). Stimulus order was randomized with a 2 s interval between each presentation.

Data Analysis

Data processing includes four parts: widefield imaging analysis for identifying the location of somatosensory and auditory cortices in the chronic window; two-photon imaging analysis for acquiring neuronal activity from fluorescent brightness during the stimuli; registration for identifying the location of individual fields of view within the entire window; response analysis for calculating the response to any given stimulus. Many of these methods have been described in a previously published paper (Issa et al., 2014) but will also be described in detail here.

Widefield Imaging Analysis

On a pixel-by-pixel basis, the baseline fluorescence signal F_0 was taken as the average image brightness across the 10 frames directly preceding the start of each stimulus, and the response was taken as the average fluorescence signal over the first 1 s (20 frames) after the start of each stimulus (F). The normalized response to each stimulus was then calculated as $\Delta F/F_0 = (F-F_0)/F_0$.

Two-Photon Imaging Analysis

We first performed a frame-by-frame image registration to correct for drift in our imaging field. Assisted by a structured sparse coding algorithm (Haeffele et al., 2014), we then performed a semiautomatic segmentation of our movies acquired from a two-photon imaging session to acquire regions-of-interest (ROIs) corresponding to individual neurons. From each ROI, we generated brightness-over-times (BOTs). This process included neuropil subtraction, where we subtracted the signal from pixels within 75 μm of each cell (but excluding pixels containing other cell bodies). Using a low-pass filter, a smooth baseline (F_0) was fit to each BOT, allowing for calculation of a normalized fluorescence signal $\Delta F/F_0$. To increase the temporal accuracy of our Ca^{2+} signal and to decrease the influence of noise, we employed a non-negative deconvolution method with a time constant of 0.7 s to generate a correlate of spike probability (Vogelstein et al., 2010), which was then thresholded to estimate events per time bin, which loosely corresponds to the frequency of spikes or firing rates for a given neuron. Events per time bin was used for constructing tuning curves and other measures as described in the section of "Response Analysis."

Registration

For most mice, the window was initially mapped under two-photon imaging by tiling z-stacks across the entire visible window. This process involved acquiring images at multiple depths (from dura down to 300 or 400 μm below dura in 50 or 100 μm steps) at high resolution (1024x1024 pixels for each 465x465 μm^2 field). Two-photon imaging fields were registered to widefield imaging fields by using vasculature landmarks. Information about the location of auditory (AI, AII, and AAF) and somatosensory cortices (S1, S2, and ISF) obtained from widefield imaging was then used to identify which cortical field each two-photon imaging field belonged to.

Response Analysis

Response analysis includes five major parts: (1) event rate normalization; (2) quality measure of responsiveness; (3) best frequency extraction; (4) construction of tuning curves; (5) calculation of sound-driven response change; (6) statistical test for verifying whether ratio of bandpass neurons in S1 is significantly smaller than ratio of highpass neurons in S2.

For event rate normalization, we used a 600-ms period after the start of a stimulus as our response window. The averaged baseline-corrected signal during that period yielded the event rate or response for each individual stimulus.

We used three indices to measure the responsiveness of a neuron: (1) the total area under the tuning curve (tc_1); (2) the *p*-value (tc_2) of N-way ANOVA to quantify whether there is a significant difference between the responses across different stimuli frequencies, which indicates a neuron is tuned to stimulus frequency; (3) the ratio (tc_3) of the averaged response during the response window divided by the average response outside the response window, a measure of driven rate. Each quantity was passed through a function with a saturating nonlinearity and summed to yield a unitless measure of responsiveness *qm*:

$$qm = 1.8 \times \tanh\frac{tc_1 - 20}{15} + \tanh(2 \times log_{10}(0.05/tc_2)) + \tanh(1.4 \times (tc_3 - 1.8))$$

This ad hoc measure was thresholded to categorize neurons as responsive or not responsive to a particular stimulus type. Individual neurons were carefully scrutinized to test for the adequacy of this approach. Also, adjustments in the threshold did not appreciably alter the results reported in this work. For further analysis, if the neuron responded only to tactile stimuli, we classified it as a tactile-selective neuron. Similarly, if the neuron only responded to any of the sound stimuli we tested, we classified it as a sound-selective neuron.

Extracting the best tactile frequency is very important for separating bandpass and highpass neurons. We used two different approaches to measure best frequency: 1) the weighted average of all the significant responses; 2) the frequency that gives the maximum response. We averaged these two measures to get the best frequency. Neurons with best frequencies less than or equal to 60 Hz are categorized as bandpass neurons while neurons with best frequencies greater than 60 Hz are categorized as highpass neurons.

To construct tuning curves, we used two different strategies. For characterizing tuning properties of tactile-selective neurons in S1 and S2 (Figure 3), we normalized the response for different tactile frequencies to the maximum response among all the tactile frequencies. For characterizing the sound modulation effect of response to tactile stimuli (Figure 4-7), we normalized the response to the maximum response of either tactile stimuli or tactile plus auditory stimuli.

To get the sound-driven response change of tactile stimuli (Figure 4-6), we calculated the ratio of response change (ΔR) as the sum of response change at each frequency divided by sum of responses to both tactile alone and tactile plus auditory stimuli.

To test whether the fraction of bandpass neurons in S1 (p_1) is significantly smaller than the fraction of bandpass neurons in S2 (p_2), we first had a null hypothesis H_0: $p_2 \leq p_1$. Then we used two-proportion z-test and calculated the z-score as following:

$$Z = \frac{p_1 - p_2}{\sqrt{p_0(1-p_0)(\frac{1}{N_1} + \frac{1}{N_2})}}$$

in which,

$$p_0 = \frac{n_1 + n_2}{N_1 + N_2}$$

n_1 is the number of bandpass neurons in S1, N_1 is the number of total tactile responsive neurons in S1; n_2 is the number of bandpass neurons in S2, N_2 is the number of total tactile responsive neurons in S2. After calculating the z-score for the hypothesis H_0, we obtained the *p*-value associated with the z-score according to the standard normal distribution. If $p < 0.05$, we reject the hypothesis H_0, otherwise, we accept the hypothesis. In other words, if $p < 0.05$, we would conclude that the fraction of bandpass neurons in S2 (p_2) is significantly larger than the fraction of bandpass neurons in S1 (p_1).

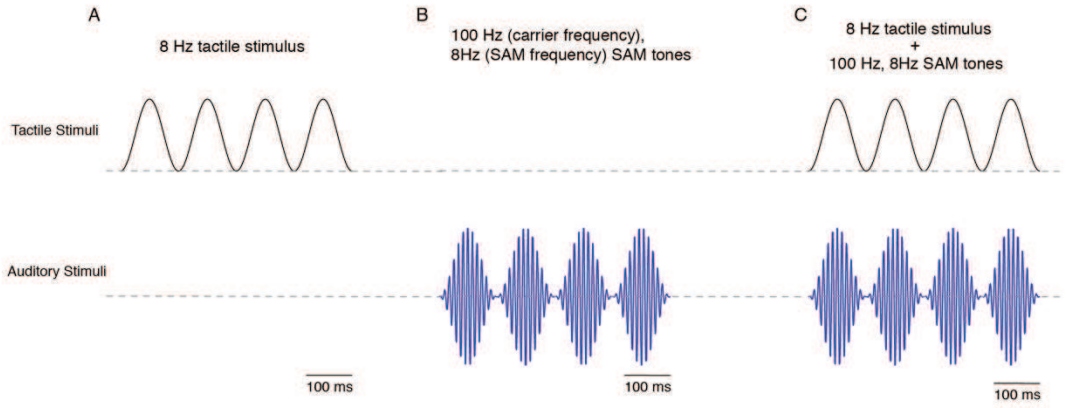
A
8 Hz tactile stimulus
B
100 Hz (carrier frequency),
8Hz (SAM frequency) SAM tones
C
8 Hz tactile stimulus
+
100 Hz, 8Hz SAM tones
Tactile Stimuli
Auditory Stimuli
100 ms
100 ms
100 ms

Figure 1. Schematic Waveforms for Three Different Stimuli

(A) Tactile stimulation alone, illustrated by a waveform of an 8 Hz sinusoidal tactile stimulus with a 500 ms stimulus period. 100 ms scale bar shown at the bottom right.

(B) Sound stimulation alone, illustrated by a waveform of 100 Hz (carrier frequency), 8 Hz (SAM frequency) SAM tones, again with a 500 ms stimulus period.

(C) Combined auditory-tactile stimulation, with simultaneous presentation of tactile (top) and auditory (bottom) stimuli. Here the 8 Hz frequency of the tactile stimulus is matched with the SAM frequency of the sound stimulus.

CHAPTER 3

Results

Widefield Ca^{2+} Imaging Reveals Tactile and Auditory Responsive Areas of Mouse Neocortex

We first performed widefield imaging of the left temporal lobe of mouse neocortex to identify regions that respond to either tactile or auditory stimuli individually. Transgenic mice expressing the Ca^{2+}-indicator GCaMP6s under pan-neuronal promoters (Dana et al., 2014; Madisen et al., 2015; Wekselblatt et al., 2016) were implanted with a chronic cranial window exposing up to 5 ø mm of the left hemisphere (Issa et al., 2014). This approach allows us to capture the majority of the auditory cortex along with the primary somatosensory (S1), the secondary somatosensory (S2), and the insular somatosensory (ISF) cortices all in the same window. Mice were habituated to head fixation while running on a spherical treadmill. During widefield fluorescence imaging, either tactile stimuli (piezo-driven movement with specific frequencies) or auditory stimuli (sinusoidal amplitude modulated (SAM) tones) were delivered to the contralateral-side target whisker or ear, respectively (Figure 2A). In response to a sinusoidal 128 Hz tactile stimuli of the C2 whisker, we observed rapid fluorescent transients at three distinct locations (Figure 2B, 2C). A spatial map of these changes, as shown in Figure 2D, highlights the locations of the three responsive loci. Based on stereotaxic coordinates and intrinsic imaging, the most medial locus was identified as S1, the middle locus corresponded to S2, and the most lateral locus corresponded to ISF. Although the magnitude of the transient in ISF was smaller than S1 or S2, the kinetics of the responses were similar among all three regions (Figure 2B). While the auditory cortex was largely quiescent, we observed a small transient in the anterior auditory field (AAF) (Figure 2C). However, as AAF is in proximity to ISF (Figure 2H), the spatial resolution of widefield imaging is insufficient to

distinguish the two regions conclusively. On the other hand, in response to auditory stimuli composed of SAM tones across sixteen different carrier frequencies covering the whole hearing range (3 to 96 kHz) of mice, we observed significant fluorescent responses in regions corresponding to the auditory cortex (the primary auditory cortex (AI), the secondary auditory cortex (AII), and AAF) (Figure 2F, 2G). Interestingly, we also observed small transients in the somatosensory areas, especially in S2 and ISF, highlighting possible cross-modal interaction (Figure 2E).

Somatosensory Neurons are Tuned to the Frequency of Tactile Stimuli

Having verified the location of each cortical area within our cranial window, we next examined the responses of individual neurons located in layer 2/3 across various somatosensory regions. Using two-photon Ca^{2+} imaging, we can simultaneously monitor the activity of hundreds of neurons within a field of view spanning 465×465 μm^2, a region sufficiently large to include the C2 barrel column in S1 (Figure 3A) (Peron et al., 2015). To measure evoked tactile responses, we chose sinusoidal piezo-driven tactile stimuli with frequencies ranging from 2 to 128 Hz presented in random order. The upper limit of 128 Hz was chosen to avoid any piezo-generated sound within the hearing range of mice (see Methods). We found that 18% of neurons in S1 were responsive to tactile stimuli. By comparison, a previous study found 37% of S1 neurons were responsive for tactile task-related responses (Kwon et al., 2016). For two exemplar S1 neurons, Figure 3B displays individual baseline-normalized fluorescent responses ($\delta\hat{F} = \Delta F/F_0$) to tactile stimuli from multiple trials (gray) and their ensemble average (black) sorted according to stimulus frequencies. A normalized tactile response (*NTR*) for each stimulus was then estimated as the ratio of the mean fluorescence change ($\delta\hat{F}_{mean}(i)$) for the given stimulus (i) to the maximal

fluorescence change ($\max_i \delta \hat{F}_{mean}(i)$) observed across all stimuli. Plotting the normalized tactile response as a function of the stimulus frequencies revealed a normalized tactile tuning curve (Figure 3C). Upon scrutinizing many such tactile tuning relations, we found that neurons can be classified into two categories, namely "bandpass" or "highpass" according to their response properties (Figure 3C). The bandpass neurons have biphasic tuning curves (Figure 3C, left) while the highpass neurons exhibit monotonically increasing response characteristics (Figure 3C, right). Practically, the best tactile frequency (*BTF,* see Methods*)* served as a convenient discriminator for the two neuronal classes. Figure 3D shows the overall distribution of *BTF* for tactile-responsive neurons in S1. The highpass neurons appeared to outnumber bandpass neurons by 7-fold in relative prevalence.

We further assessed tactile response in neurons within S2 (Figure 3E), approximately ~ 1 mm lateral to S1 based on widefield Ca^{2+} imaging and registration (Figure 2D). We found that 8% of all neurons were responsive to tactile stimuli. Indeed, examination of tactile tuning curves revealed the presence of neurons with both bandpass (left, Figure 3F,3G) and highpass (right, Figure 3F,3G) response characteristics. Interestingly, we found that bandpass neurons were more prevalent in S2 compared to S1 (Figure 3H; $p < 0.01$, see Methods). The highpass neurons nonetheless outnumbered bandpass neurons by ~4-fold. The coarse similarity in response characteristics of both S1 and S2 neurons indicates that tactile frequency tuning may be a general feature for decoding tactile sensation in multiple regions of the somatosensory cortex.

Simultaneous Auditory Input Modulates Tactile Responses in S2

To systematically identify possible multimodal integration, we explored whether concurrent auditory stimuli could modify tactile responses in the somatosensory cortex, focusing initially on

S2 given its putative role in higher-order tactile processing (Jones and Powell, 1970; Lemus et al., 2010) (Figure 4A). Accordingly, we quantified fluorescence changes of single neurons in S2 in response to three distinct stimulus conditions: (1) tactile stimuli alone, (2) auditory stimuli (SAM tones) alone, and (3) tactile and auditory stimuli presented concurrently. Figure 4B-E displays responses for two tactile-selective neurons within a single field-of-view demonstrating two multisensory effects. Neuron 1 exhibited robust highpass tactile tuning responses (black, Figure 4B) that were unperturbed upon simultaneous presentation of acoustic and tactile stimuli (red, Figure 4B). The normalized responses obtained with tactile stimuli alone and with concurrent tactile and auditory stimuli are overlaid in Figure 4C to facilitate comparison. The responses here were normalized to the maximal fluorescence change observed with either tactile or simultaneous tactile and auditory stimuli. By contrast, neuron 2 exhibited robust bandpass responses when probed with tactile stimuli alone (black, Figure 4D) but was largely nonresponsive when both tactile and auditory stimuli were presented concurrently (red, Figure 4D). Overlay of normalized tactile responses in Figure 4E across a broad range of tactile stimulus frequencies in the presence (black) and absence (red) of sound illustrates the dramatic sound-driven inhibition observed in neuron 2. Of note, both neurons 1 and 2 were nonresponsive to sound stimuli altogether (blue, Figure 4B, 4D). Further survey of neurons in S2 revealed that for some neurons their tactile responses were facilitated by sound (Figure 4F, black bars; Figure 6D-F). These results illustrate a powerful mode of multisensory processing whereby the response of individual cortical neurons to their primary sensory modality is modulated by a concurrent secondary sensory input.

How prevalent is sound modulation of tactile responses in S2? A distinctive advantage of two photon Ca^{2+} imaging is its ability to simultaneously assess changes in neuronal function at both the level of an individual cell as well as for a population of cells. Consequently, for all tactile-

selective neurons in S2, we systematically probed for statistically significant changes in tactile responses when evoked concurrently with auditory stimuli using N-way ANOVA test with a pre-established criterion ($p < 0.05$). We found that only 45% of highpass neurons and 27% of bandpass showed no change in tactile responses with concurrent sound stimuli (Figure 4F). Furthermore, to probe the overall potency of sound modulation, we quantified the net change in aggregate tactile responses (average response elicited across all tactile frequencies) when evoked by simultaneous tactile and auditory stimuli (ΔR) (Figure 4G). Characterized accordingly, we found amongst all bandpass neurons 71% were inhibited while 2% were facilitated (Figure 4F). Amongst highpass neurons, we found 48% were inhibited while 6% were facilitated (Figure 4F). Moreover, the relative strength of sound-driven inhibition was more potent in bandpass neurons ($\Delta R = 45\%$) in comparison to highpass neurons ($\Delta R = 30\%$; $p < 0.01$) (Figure 4G). In this manner, sound-driven inhibition appeared to be both more prevalent and prominent in bandpass neurons, indicating a possible tactile frequency-dependence in multisensory interactions.

Concurrent Auditory Input Modulates Tactile Responses in S1

Traditionally, primary sensory cortices are believed to be predominantly involved in unimodal processing with the presence of multimodal interactions long-debated. While a few studies have illustrated potential multisensory interactions in the primary cortices (Brosch et al., 2005; Foxe et al., 2002; Kayser et al., 2005), others have argued that multisensory integration is largely restricted to higher-order cortices (Lemus et al., 2010). Armed with our ability to systematically dissect multisensory modulation, we next examined whether tactile responses in S1 are modulated by concurrent auditory stimuli. Figure 5A-G show the fluorescence recordings for three individual tactile-selective neurons within a single field-of-view in response to tactile stimuli alone or

concurrent tactile and auditory stimuli. Neuron 1 exhibited minimal change to its tactile tuning relation following addition of simultaneous auditory stimuli (Figure 5B, 5C). By contrast, tactile responses of both neurons 2 and 3 were inhibited by auditory stimuli (Figure 5D–5G), with the bandpass neuron 3 exhibiting stronger inhibition than the highpass neuron 2. Notably all three neurons were non-responsive to acoustic stimuli when presented alone (blue traces, Figure 5B, 5D, 5F). At the population level, unlike neurons in S2, the tactile responses for a majority of highpass (63%) and bandpass (53%) neurons in S1 were unaltered by auditory stimuli. Nonetheless, we identified a substantial number of tactile neurons exhibiting sound-driven inhibition and a small number with sound-driven facilitation (Figure 6A-C). The overall proportion of both bandpass and highpass neurons exhibiting sound-modulation of tactile responses is summarized in Figure 5H. Like sound-modulated neurons in S1, the degree of inhibition appeared to be stronger with bandpass compared to highpass neurons ($p < 0.01$), while the degree of sound-driven facilitation appeared to be similar between the two types of tactile neurons (Figure 5I). These results unambiguously establish the presence of multisensory modulation of neurons in the primary somatosensory cortex. Despite subtle differences, sound-driven modulation of tactile responses in both S2 and S1 neurons appears to follow a similar pattern, suggesting that multimodal integration may be more widespread in the cortex than previously thought.

Sound-Driven Inhibition of Tactile Neurons Preferentially Alters Low Frequency Responses

Given the wide prevalence of sound-driven inhibition of tactile responses observed for neurons in the somatosensory cortex, we next sought to dissect spectral features of multimodal processing. Consequently, we scrutinized tactile tuning relations in the presence and absence of simultaneous auditory stimuli for four distinct neurons with varying *BTF* all within a single field-of-view.

Neuron 1 exhibiting bandpass tactile frequency tuning with a low *BTF* was inhibited across all responsive tactile frequencies (i.e. 8 – 32 Hz) (Figure 7A, 7B). Interestingly, for neurons 2 and 3, sound-driven inhibition was nearly complete at low tactile frequencies (below 32 Hz) while the high-frequency tactile responses were largely spared. Similar effects were also observed for neuron 4 with high-pass tactile tuning properties, suggesting that sound-driven modulation is exquisitely dependent on the frequency of tactile stimulation. Responses to low-frequency tactile stimuli are preferentially suppressed while response to high-frequency tactile stimuli are preserved.

To quantitatively assess tactile spectral properties of sound-driven modulation, we clustered neurons into five categories according to their best tactile frequencies (Figure 7C). Normalized tactile tuning curves (Figure 7C) in the absence (black) and in the presence (red) of concurrent sound stimuli were averaged for the five categories. Sound-driven inhibition of tactile responses was apparent for all five neuronal categories. To quantify the strength of sound-driven inhibition, we computed the ratio of normalized tactile responses in the presence of sound stimuli to those in the absence at each individual tactile frequency (r_{sound}). For all five neuronal categories, r_{sound} increased monotonically with increasing tactile stimulus frequency. Here, the low frequency tactile responses were strongly diminished ($r_{sound} \sim 0.2$) by sound stimuli while high frequency tactile responses were minimally perturbed ($r_{sound} \sim 1$) (Figure 7D). The tactile frequency for half-inhibition ($TF_{1/2}$) increased only weakly as a function of the best tactile frequency (*BTF*) for the given class of neurons (Figure 7G). Overall, these results show that sound-driven inhibition exquisitely depends upon tactile stimulus frequency with low frequency tactile stimuli preferentially suppressed.

This spectral dependence of sound-modulation of tactile responses has two distinct functional consequences. First, the preferential sound-driven inhibition at low tactile frequencies

results in a rightward shift in the overall tactile tuning relation for individual neurons. This effect manifests as a positive change in *BTF* for a majority of neurons (Figure 7E). Second, the overall inhibition of tactile responses is higher for neurons with low *BTF* (Figure 7F).

Sound-Selective Neurons in S2 but not Auditory Cortex Are Suppressed by Touch

Alongside touch-selective neurons in S2, we observed a small but reliable population of sound-selective neurons (1.2% of all S2 neurons recorded) that responded to auditory stimuli but not to tactile stimuli. We selected sound-selective neurons that were responsive to the auditory stimuli used in the combined stimuli, then we examined whether tactile stimulation could alter their response to sound. Shown in Figure 8A-C are the responses of an exemplar sound-selective neuron located in S2. This neuron did not respond to tactile stimuli at any frequency (Figure 8B, black traces) but did respond to sound alone (Figure 8B, blue trace). When the same sound was paired with different tactile frequencies, the sound response was almost completely abolished at the highest tactile frequencies (Figure 8B, red traces). The normalized tuning curves clearly demonstrate this tactile frequency-dependent suppression of sound responses in this neuron (Figure 8C). This trend was observed for the population-averaged tuning curve of selected neurons in S2 (Figure 8D), with suppression occurring for tactile frequencies above 32 Hz. The ratio of the averaged response to sounds paired with high frequency (104-128 Hz) tactile stimulation versus the averaged response to sounds paired with low frequency (2-22 Hz) tactile stimulation (r_{tactile}) provided a convenient measure of this suppression. The distribution of these values for sound-selective S2 neurons, shown in Figure 8E, shows that sound responses in most neurons were suppressed by high frequency tactile stimuli.

To ascertain whether this effect was specific to S2, we measured the effect of tactile stimulation on the responses of sound-selective neurons in auditory cortex. As for S2, we limited our analysis to neurons that responded to the auditory stimuli we used in the combined stimuli. Shown is an exemplar neuron that responds to sound alone but not to touch. The addition of tactile stimulation at any frequency did not change the response of this neuron to sound (Figure 8F-H). Across the population of selected neurons in auditory cortex, neurons did not exhibit a tactile-frequency dependent change in their sound response (Figure 8I-J). In stark contrast to S2, the mean response ratio (r_{tactile}) in auditory cortex is nearly 1 (Figure 8K).

Clustering of Sound-Selective Neurons in S2

We next examined whether sound-selective neurons were spatially clustered among the population of tactile-selective neurons in S2. For all imaging fields that contained both types of neurons, we computed the distance between all pairs of responsive neurons in S2. The distribution of these pairwise distances is shown in Figure 9A. Next, we computed the distance between sound-selective neurons and tactile-selective neurons in S2 (Figure 9B). We observed an increased average distance of 36 μm for the distance between sound-selective and tactile-selective neurons (Figure 9B, blue) versus the distance between all pairs of responsive neurons (Figure 9B, black). This result provides evidence for a small amount of clustering of sound-selective neurons in S2.

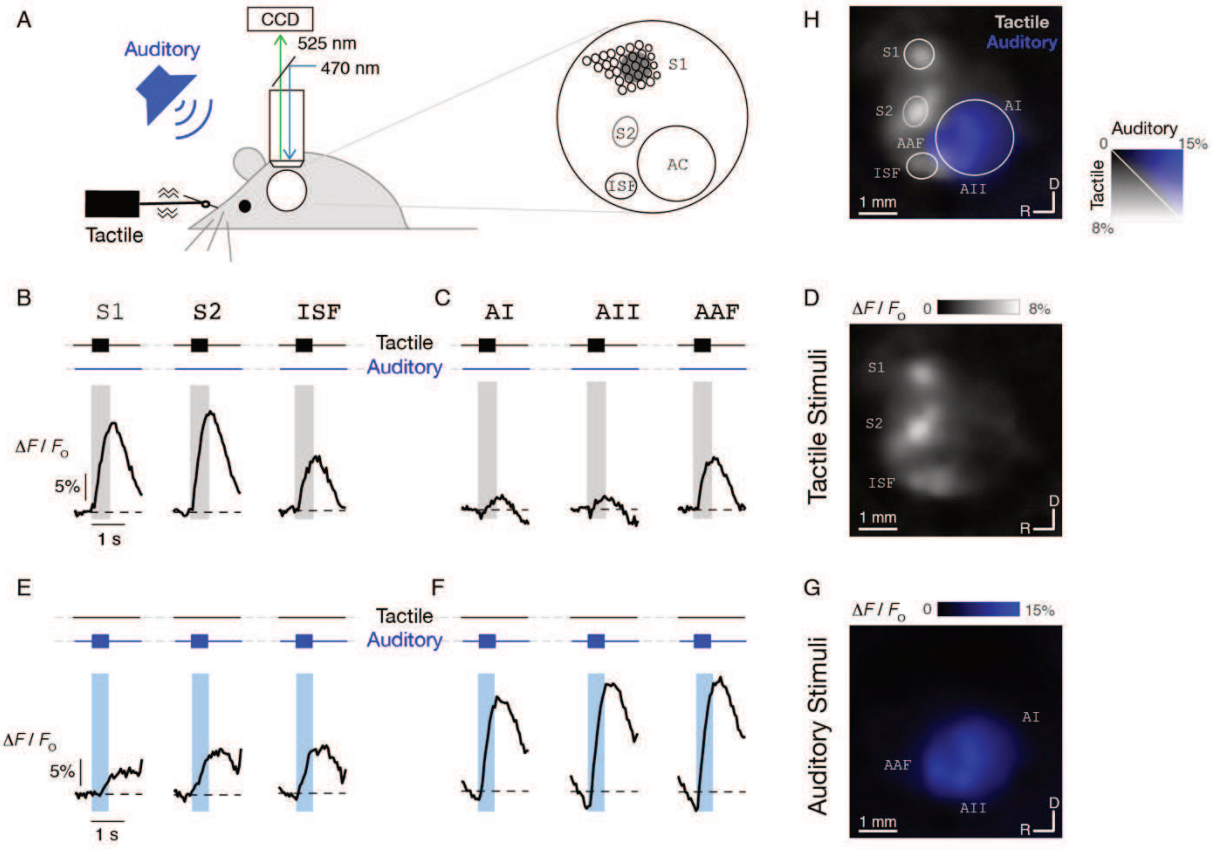
A
Auditory
CCD
525 nm
470 nm
Tactile
S1
S2
AC
ISF
H
Tactile
Auditory
S1
S2
AI
AAF
ISF
AII
1 mm
D
R
Auditory
0
15%
Tactile
8%
B
S1
S2
ISF
C
AI
AII
AAF
Tactile
Auditory
ΔF / F0
5%
1 s
D
ΔF / F0
0
8%
Tactile Stimuli
S1
S2
ISF
1 mm
D
R
E
F
Tactile
Auditory
ΔF / F0
5%
1 s
G
ΔF / F0
0
15%
Auditory Stimuli
AI
AAF
AII
1 mm
D
R

Figure 2. Responses to Tactile and Auditory Stimuli under Widefield Ca^{2+} Imaging

(A) Widefield imaging set-up. Tactile and auditory stimuli are delivered to a head-fixed awake mouse. Piezo coupled to right C2 whisker provides vibration in rostral-caudal direction while speaker delivers sinusoidal amplitude-modulated (SAM) tones to the right ear. 5 ø mm chronic cranial window over the left temporal cortex (white circle) spans somatosensory and auditory cortical areas. GCaMP6s fluorescence (470 nm illumination and 525 nm emission) collected by CCD camera through 4× objective.

(B) Responses to tactile stimuli in somatosensory areas. Single-trial Ca^{2+} transients evoked in S1, S2, and ISF in response to 128 Hz whisker stimulation. Black trace shows fluorescence activity $(\Delta F/F_0)$ averaged over 68x68 μm^2 regions in each of these three areas. Vertical gray bar represents 500 ms stimulus period. Black squares represent presentation of tactile stimuli.

(C) Responses to tactile stimuli in auditory areas. Same format as B.

(D) Ca^{2+} activity during presentation of tactile stimuli reveals location of somatosensory areas. Spatial map depicts average response to 12-128 Hz tactile stimuli, taken as average $\Delta F/F_0$ over first 1 s after stimulus onset. Responsive regions correspond to S1, S2, and ISF, as labeled. Dorsal-rostral orientation and 1 mm scale bar shown at bottom.

(E) Responses to 15.1 kHz, 10 Hz SAM tone stimuli in S1, S2 and ISF. Same format as B with vertical blue bar representing 500 ms stimulus period. Blue squares represent presentation of SAM tones.

(F) Responses to 15.1 kHz, 10 Hz SAM tone stimuli in auditory areas. Same format as E. The fluorescence signal ($\Delta F/F_0$) decreases in the period immediately before the start of each auditory stimulus. This behavior occurs because the fluorescence signal has not fully recovered from the preceding stimulus and is still decaying back to the true baseline value. Tactile responses (panels B and C) do not exhibit this feature because responses to tactile stimuli are smaller and sparser (fewer tactile frequencies evoked responses compared to sound stimulation), thus allowing the transients in response to the preceding stimuli to decay more closely to baseline.

Comparing with tactile response in panel B and C, we noticed that fluorescence signal $\Delta F/F_0$ decreases before the auditory stimulus starts. This is because $\Delta F/F_0$ haven't fully recovered from previous stimulus. Tactile responses don't have this feature (panel B and C), because the $\Delta F/F_0$ for tactile stimulus is smaller and fewer frequencies would evoke responses. So, the transient for previous stimulus is more easily to recover to the baseline.

(G) Ca^{2+} activity during presentation of auditory stimuli reveals location of auditory areas. Image shows average response of 3-19.0 kHz, 10 Hz SAM tone stimuli. Responsive regions correspond to AI (primary auditory cortex), AII (secondary auditory cortex), and AAF (anterior auditory field), as labeled. Same format as D.

(H) Overlay of responses to tactile (gray, as shown in D) and auditory (blue, as shown in G) stimuli highlighting relative location of somatosensory and auditory fields in the same window. Rostral-caudal orientation and $\Delta F/F_0$ scale bar shown at bottom right.

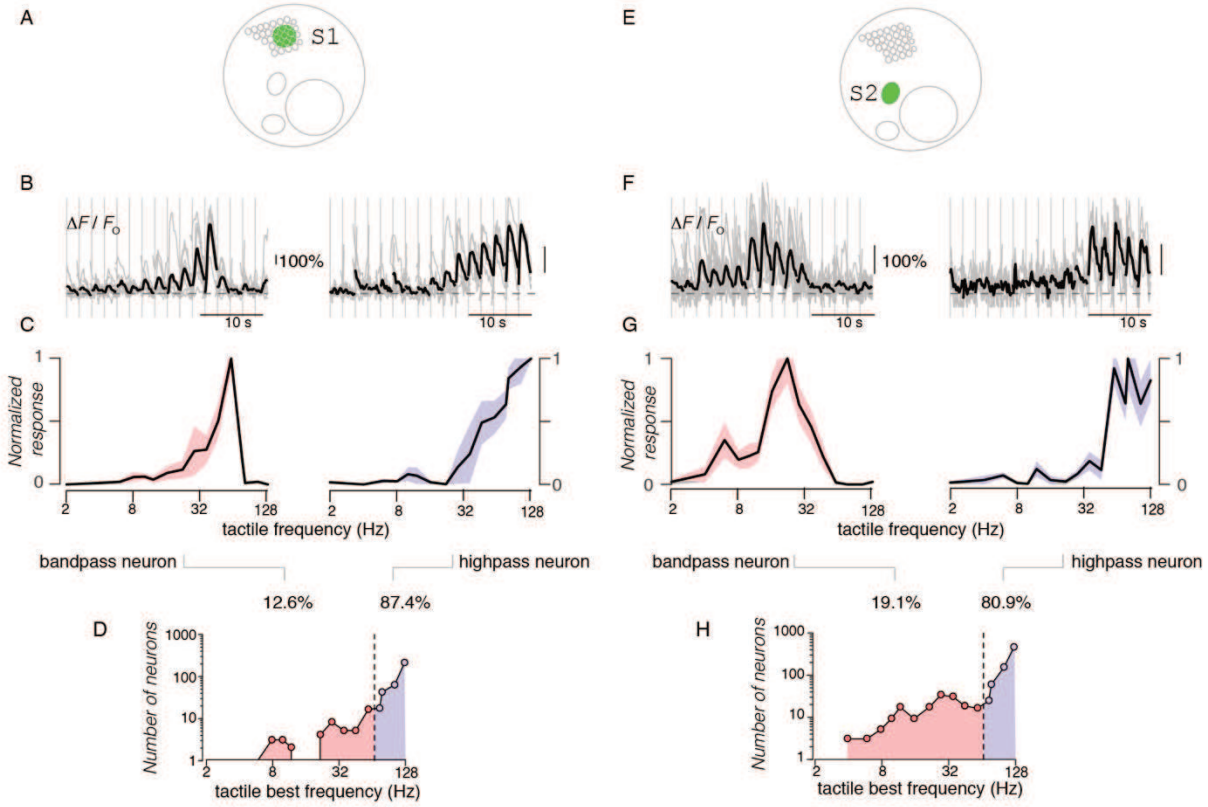
A
S1
E
S2
B
F
ΔF / Fo
100%
10 s
C
G
Normalized response
tactile frequency (Hz)
bandpass neuron
highpass neuron
12.6%
87.4%
19.1%
80.9%
D
H
Number of neurons
tactile best frequency (Hz)

Figure 3. Responses to Tactile Stimuli in Somatosensory Cortices under Two-Photon Ca^{2+} Imaging

(A) Schematic highlights location of field-of-view (FOV) centered on C2 barrel within S1.

(B) Ca^{2+} activity ($\Delta F/F_0$) of two exemplar S1 neurons during presentation of tactile stimuli at different frequencies. Stimuli were played in random order and responses sorted by increasing frequency (2-128 Hz). Gray traces show $\Delta F/F_0$ for individual trials. Black traces show average $\Delta F/F_0$ across all trials. Vertical gray line denotes start of each stimulus. These exemplars depict typical bandpass (left) and highpass (right) neurons observed.

(C) Frequency tuning curves of individual neurons shown in B. Responses are averages over a 600 ms period of the deconvolved $\Delta F/F_0$ traces, which are then normalized to the maximum response across all stimuli. Standard error shown as shaded region. Frequency of tactile stimuli shown on the *x*-axis.

(D) Population distribution of best tactile frequencies (*BTF,* see Methods) for S1 neurons. Black circles show number of neurons tuned to each frequency tested. Neurons with best frequencies lower than 60 Hz were categorized as bandpass neurons (pink, 12.6% of responsive tactile neurons in S1) while those with best frequencies above 60 Hz were categorized as highpass neurons (blue, 87.4% of responsive tactile neurons in S1). Both *x* and *y* axes plotted on a logarithmic scale.

(E) Schematic depicting location of S2.

(F) Ca^{2+} activity induced by tactile stimuli in S2 for two exemplar neurons, again showing bandpass (left) or highpass (right) behavior. Same format as B.

(G) Frequency tuning curves for the exemplar neurons shown in F. Same format as C.

(H) Population distribution of best tactile frequencies (*BTF*) in S2. Now 19.1% of responsive neurons in S2 were bandpass neurons (pink) and 80.9% were highpass neurons (blue). Same format as D.

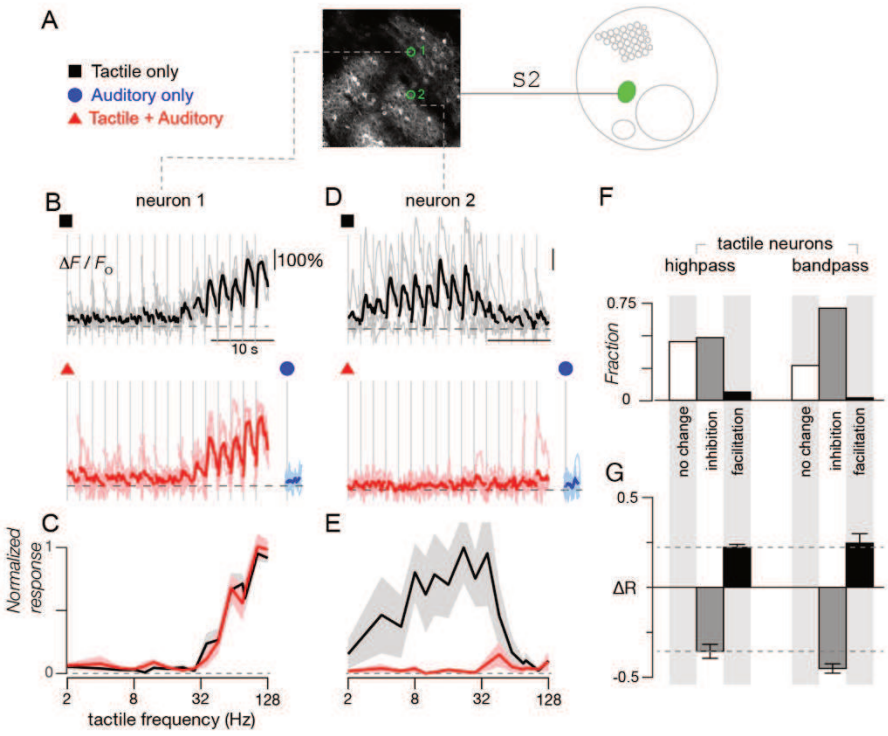
A
Tactile only
Auditory only
Tactile + Auditory
1
2
S2
B
neuron 1
ΔF / F0
100%
10 s
D
neuron 2
C
Normalized response
1
0
2
8
32
128
tactile frequency (Hz)
E
2
8
32
128
F
tactile neurons
highpass
bandpass
Fraction
0.75
0
no change
inhibition
facilitation
no change
inhibition
facilitation
G
0.5
ΔR
-0.5

Figure 4. Sound Modulated Response to Tactile Stimuli in S2

(A) Baseline fluorescence image of two-photon imaging field (middle) located in S2, as illustrated in schematic map (right). Symbols (left) denote different stimuli tested. Exemplar neurons to be scrutinized in panels B-E are highlighted by green circles (middle panel).

(B) Responses of exemplar neuron to tactile stimuli alone (black traces, top panel) or to combined tactile and auditory stimuli (red traces, bottom panel). In both cases, tactile frequency ranged from 2 to 128 Hz. For the combination stimulus, a concurrent auditory stimulus (10 kHz, 40 Hz SAM tones at 40 dB attenuation) was added to the tactile stimuli. In addition, blue traces (bottom right) show averaged responses to 10 kHz, 16 Hz SAM tones and 10KHz, 32 Hz SAM tones at 40 dB attenuation. For all cases, individual trials shown as light traces and response averages shown as dark traces.

(C) Frequency tuning curves of the normalized response to tactile stimuli and combined tactile plus auditory stimuli for exemplar neuron shown in B. Black line shows the normalized tuning curve for responses to tactile stimuli. Red line shows the normalized tuning curve for responses to tactile plus auditory stimuli. Standard error shown as shaded gray and pink regions.

(D) Exemplar neuron from the same imaging field as neuron 1, now exhibiting complete suppression of its response for combined tactile and auditory stimuli. Same format as B.

(E) Tuning curves of the normalized response to tactile stimuli and tactile plus auditory stimuli for exemplar neuron 2 from panel D.

(F) Fraction of neurons in S2 exhibiting either no change, a decrease (inhibition), or an increase (facilitation) when SAM tones were added to the tactile stimuli. Criteria determined by ANOVA ($p < 0.05$). Neurons were categorized as either highpass (left) or bandpass (right) based on their best tactile frequency (*BTF*). Among all the tactile responsive highpass neurons, 306 neurons have no change, 328 neurons get inhibited, and 43 neurons get facilitated during the combined stimuli. However, among all the tactile responsive bandpass neurons, 43 neurons have no change, 114 neurons get inhibited, and 3 neurons get facilitated during the combined stimuli.

(G) Percentage change in response of S2 neurons to tactile stimuli (ΔR) when SAM tones were added. Neurons were divided into highpass (left) and bandpass (right) neurons that showed either a decrease (gray) or increase (black) in their response, as indicated in panel F. Error bars show the standard error of ΔR among inhibited or facilitated neurons.

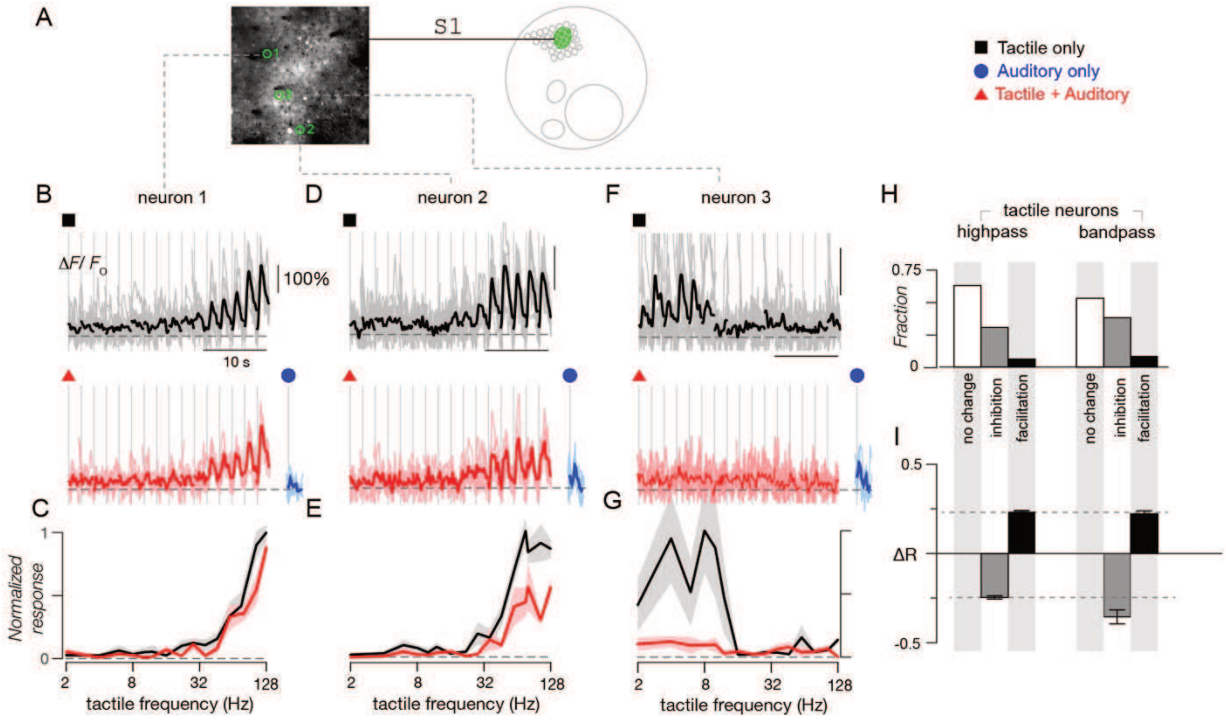
A
S1
o1
o3
o2
Tactile only
Auditory only
Tactile + Auditory
B
neuron 1
D
neuron 2
F
neuron 3
ΔF/ F0
100%
10 s
C
E
G
Normalized response
tactile frequency (Hz)
H
tactile neurons
highpass
bandpass
Fraction
no change
inhibition
facilitation
I
ΔR

Figure 5. Sound Modulated Response to Tactile Stimuli in S1

(A) Baseline fluorescence image of two-photon imaging field (left) located in S1, as illustrated in schematic map (middle). Symbols (right) denote different stimuli tested. Exemplar neurons to be scrutinized in panels B-G are highlighted by green circles (left panel).

(B) Responses of exemplar neuron to tactile stimuli alone (black traces, top panel) or to combined tactile and auditory stimuli (red traces, bottom panel). For the combination stimulus, a concurrent auditory stimulus (10 kHz, 64 Hz SAM tones at 30 dB attenuation) was added to the tactile stimuli. Blue traces (bottom right) show averaged responses to 10 kHz, 64 Hz SAM tones alone at 30 dB attenuation.

(C) Frequency tuning curves of the normalized response to tactile stimuli and combined tactile plus auditory stimuli for exemplar highpass neuron shown in B. Same format as Figure 4C.

(D) Exemplar highpass neuron from the same imaging field as neuron 1 in panels B and C, now exhibiting suppression of its response for combined tactile and auditory stimuli. Same format as B.

(E) Tuning curves of the normalized response to tactile stimuli and tactile plus auditory stimuli for exemplar neuron 2 from panel D.

(F) Exemplar bandpass neuron from same imaging field as neurons 1 and 2, exhibiting suppression of its response for combined tactile and auditory stimuli. Same format as B and D.

(G) Tuning curves of the normalized response to tactile stimuli and tactile plus auditory stimuli for exemplar neuron 3 from panel F.

(H) Fraction of neurons in S1 exhibiting either no change, a decrease (inhibition), or an increase (facilitation) when SAM tones were added to the tactile stimuli. Criteria determined by ANOVA ($p < 0.05$). Neurons were categorized as either highpass (left) or bandpass (right) based on their best tactile frequency (*BTF*). Among all the tactile responsive highpass neurons, 205 neurons have no change, 100 neurons get inhibited, and 20 neurons get facilitated during the combined stimuli. Moreover, among all the tactile responsive bandpass neurons, 25 neurons have no change, 18 neurons get inhibited, and 4 neurons get facilitated during the combined stimuli.

(I) Percentage of change in response of S1 neurons to tactile stimuli (ΔR) when SAM tones were added. Neurons were divided into highpass (left) and bandpass (right) neurons that showed either a decrease (gray) or increase (black) in their response, as indicated in panel F. Error bars show the standard error of ΔR among inhibited or facilitated neurons.

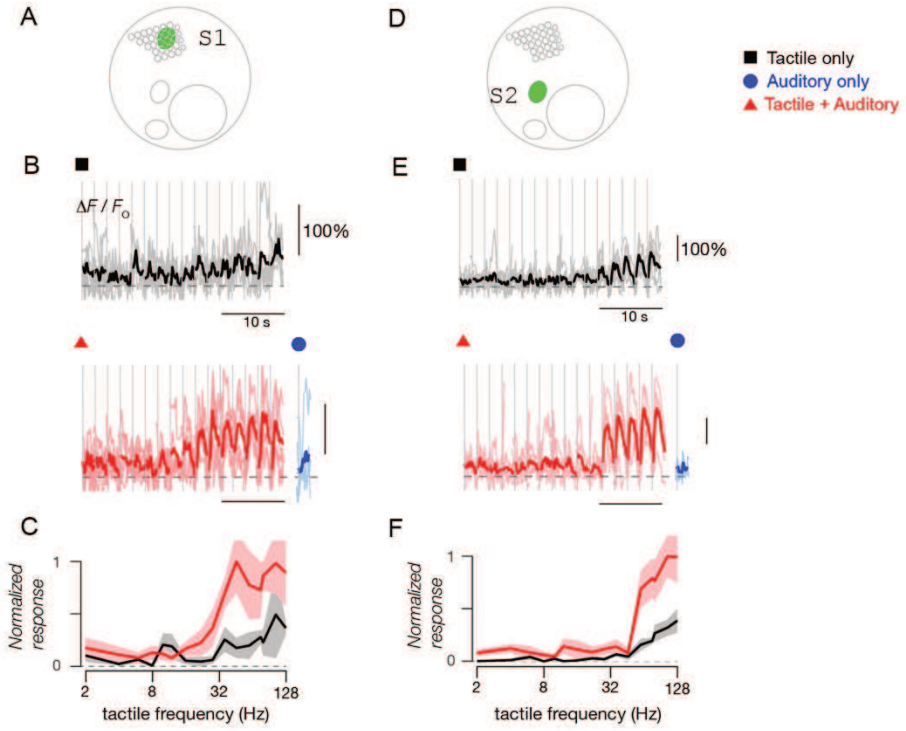
A
S1
D
S2
Tactile only
Auditory only
Tactile + Auditory
B
E
ΔF / F0
100%
10 s
C
F
Normalized response
1
0
2
8
32
128
tactile frequency (Hz)

Figure 6. Facilitation of Tactile Responses with Concurrent Sound Stimuli in Both S1 and S2

(A) Schematic highlights the location of the field-of-view (FOV) centered on C2 barrel within S1.

(B) Responses of an exemplar neuron from S1 to tactile stimuli alone (black traces, top panel) or to combined tactile and auditory stimuli (red traces, bottom panel). In both cases, tactile frequency ranged from 2 to 128 Hz. For the combined stimuli, an auditory stimulus (10 kHz, 64 Hz SAM tones at 30 dB attenuation) was delivered simultaneously as the tactile stimuli. In addition, blue traces (bottom right) show averaged responses to 10 kHz, 64 Hz SAM tones alone at 30 dB attenuation. For all cases, individual trials are shown as light traces and response averages are shown as dark traces.

(C) Frequency tuning curves of the normalized response to tactile stimuli in the absence (black) and presence (red) of concurrent auditory stimuli for exemplar neuron shown in B. Format as Figure 4C.

(D) Schematic depicts the location of S2 (left). Symbols (right) denote different stimuli tested.

(E) Responses of an exemplar neuron from S2 to tactile stimuli alone (black traces, top panel) or to combined tactile and auditory stimuli (red traces, bottom panel). For the combined stimulus, an auditory stimulus (10 kHz, 60 Hz SAM tones at 20 dB attenuation) was added to the tactile stimuli. In addition, blue traces (bottom right) show averaged responses to 10 kHz, 64 Hz SAM tones alone

at 20 dB attenuation. For all cases, individual trials shown as light traces and response averages shown as dark traces.

(F) Tuning curves show the normalized response to tactile stimuli in the presence and absence of concurrent auditory stimuli for the exemplar neuron from panel E.

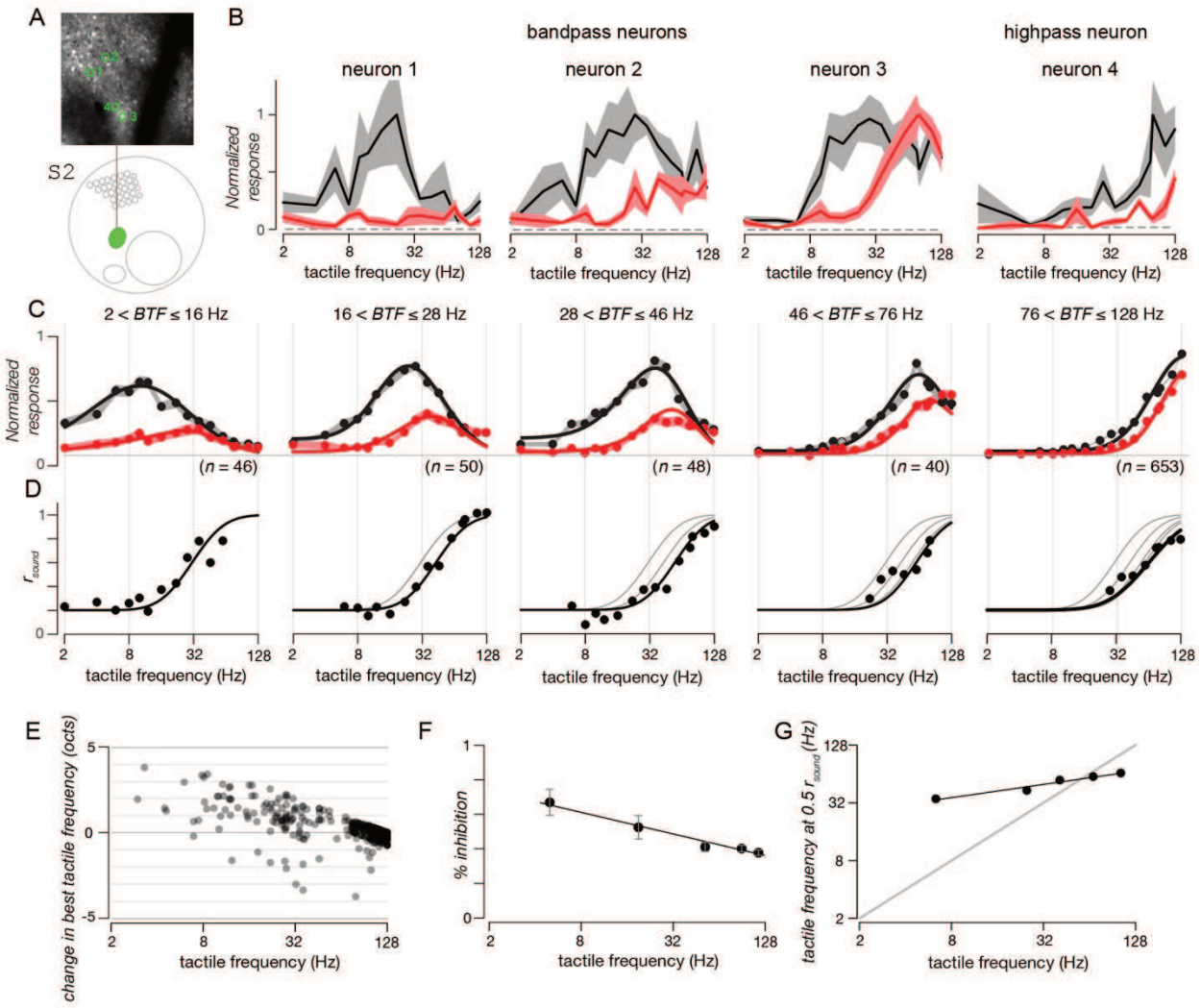
A
S2
B
bandpass neurons
highpass neuron
neuron 1
neuron 2
neuron 3
neuron 4
Normalized response
tactile frequency (Hz)
C
2 < BTF ≤ 16 Hz
16 < BTF ≤ 28 Hz
28 < BTF ≤ 46 Hz
46 < BTF ≤ 76 Hz
76 < BTF ≤ 128 Hz
(n = 46)
(n = 50)
(n = 48)
(n = 40)
(n = 653)
D
r sound
E
change in best tactile frequency (octs)
F
% inhibition
G
tactile frequency at 0.5 r sound (Hz)

Figure 7. Sound-Driven Inhibition in S2 Depends on Tactile Frequency

(A) Baseline fluorescence image of two-photon imaging field (top) located in S2, as illustrated in schematic map (bottom). Exemplar neurons to be shown in panel B are highlighted by green circles (top panel).

(B) Frequency tuning curves of the normalized response to tactile stimuli (black traces) and combined tactile plus auditory stimuli (red traces) for exemplar neurons shown in A. Standard error indicated by shaded gray (tactile alone) and pink (tactile plus auditory) regions.

(C) Population tuning curves of tactile neurons in S2 grouped by their best tactile frequency (*BTF*). Responses to tactile stimuli alone and tactile plus auditory stimuli are shown in black and red, respectively. Black circles indicate average responses at each individual frequency while solid lines show smooth fits to the tuning curves. Shaded regions represent standard error across all neurons within each specific tactile frequency domain during tactile (gray) and combined (pink) stimulation. Best tactile frequency (*BTF*) ranges used to categorize neurons are indicated above each tuning curve.

(D) Sound inhibition ratio (r_{sound}) of neurons tuned to different tactile frequencies. r_{sound} is calculated by dividing the response to tactile stimuli at each individual tactile frequency by the response to combined stimuli at each tactile frequency after subtracting the baseline (horizontal gray lines in panel C) from each. Black dots represent r_{sound} at each individual tactile frequency.

Black lines are the fitted curves for r_{sound} across 2-128 Hz. To facilitate comparison, gray lines reproduce the fitted curves of r_{sound} for neurons tuned to lower tactile frequencies.

(E) Change in best tactile frequencies of S2 neurons when sound was added (*y*-axis) as a function of best tactile frequency (*BTF*) for touch alone (*x*-axis). Each dot represents one neuron.

(F) Average percentage of inhibition of tactile-selective S2 neurons when sound is presented as a function of best tactile frequency. Each black dot represents one group of neurons tuned to different tactile frequencies as shown in C and D. Standard errors are shown in gray.

(G) Tactile frequencies at half-maximum (r_{sound} = 0.5) for neurons tuned to different tactile frequencies.

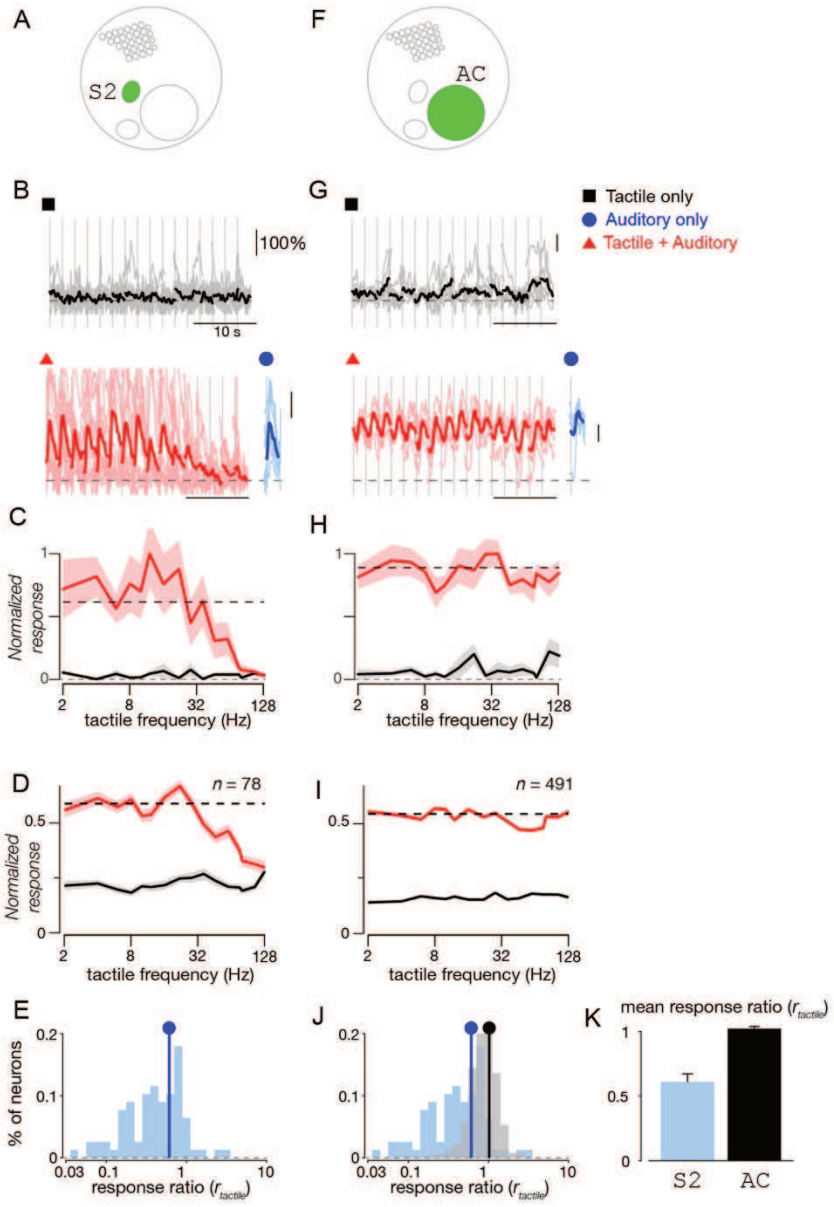
A
S2
F
AC
B
100%
10 s
G
Tactile only
Auditory only
Tactile + Auditory
C
Normalized response
tactile frequency (Hz)
H
D
n = 78
I
n = 491
E
% of neurons
response ratio ($r_{tactile}$)
J
K
mean response ratio ($r_{tactile}$)
S2
AC

Figure 8. Sound-Selective Neurons in S2 but not in AC Are Modulated by Touch

(A) Schematic map shows location of S2.

(B) Responses of exemplar sound-selective neuron to tactile stimuli alone (black traces, top panel) or to combined tactile and auditory stimuli (red traces, bottom panel). In both cases, tactile frequency ranged from 2 to 128 Hz. For the combined stimulus, a concurrent auditory stimulus (6 kHz, 10 Hz SAM tones at 20 dB attenuation) was paired with the tactile stimuli. In addition, blue traces (bottom right) show averaged responses to 6 kHz, 10 Hz SAM tones alone at 20 dB attenuation. For all cases, individual trials shown as light traces and response averages shown as dark traces.

(C) Frequency tuning curves of the normalized response to tactile stimuli and combined tactile plus auditory stimuli for exemplar neurons shown in B. Black line shows the normalized tuning curve for responses to tactile stimuli. Red line shows the normalized tuning curve for responses to tactile plus auditory stimuli. Standard error shown as shaded gray and pink regions.

(D) Averaged frequency tuning curves of the normalized response to tactile stimuli and combined tactile plus auditory stimuli for sound selective neurons in S2 that respond to the auditory stimuli used in the combined stimuli (n = 78). Standard error shown as shaded gray and pink regions.

(E) Distribution of the ratio of response at high frequency relative to low frequency for sound selective neurons in S2 shown in C. The response ratio (r_{tactile}) is calculated by dividing the

averaged response to sounds paired with high frequency (80-128 Hz) tactile stimuli with the averaged response to sounds paired with low frequency (2-22 Hz) tactile stimuli. Vertical blue line shows the average value of the response ratio ($r_{tactile}$).

(F) Schematic map shows location of AC.

(G) Exemplar neuron from auditory cortex, now exhibiting similar responses at all tactile frequencies when auditory stimuli (10 kHz, 64 Hz SAM tones at 30 dB attenuation) were added to tactile stimuli. Blue traces (bottom right) show averaged responses to 10 kHz, 64 Hz SAM tones at 30 dB attenuation. Same format as B.

(H) Frequency tuning curves of the normalized response to tactile stimuli and combined tactile plus auditory stimuli for exemplar neuron shown in G. Same format as C.

(I) Averaged frequency tuning curves of normalized response to tactile stimuli and combined tactile plus auditory stimuli for sound responsive neurons in AC that respond to the auditory stimuli used in combined stimuli (n = 491). Same format as D.

(J) Distribution of the ratio of response at high frequency relative to low frequency for sound responsive neurons in AC shown in I. Blue bars show the distribution of response ratios ($r_{tactile}$) for sound sensitive neurons in S2. Black bars show the distribution of response ratios ($r_{tactile}$) for sound responsive neurons in AC. Vertical blue line shows the average value of the response ratio ($r_{tactile}$)

of sound sensitive neurons in S2. Vertical black line shows the average value of the response ratio ($r_{tactile}$) for sound responsive neurons in AC.

(K) Mean values of ratios of response at high frequency relative to low frequency tactile stimulation for sound neurons in S2 and AC. Standard error represented by error bard.

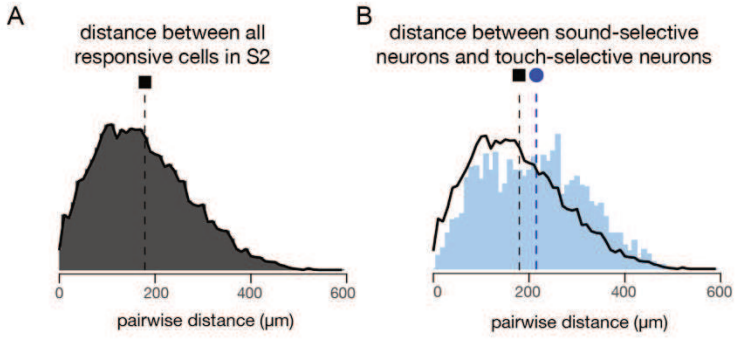
A
distance between all
responsive cells in S2
0
200
400
600
pairwise distance (μm)
B
distance between sound-selective
neurons and touch-selective neurons
0
200
400
600
pairwise distance (μm)

Figure 9. Weak Spatial Clustering of Sound-Selective Neurons in S2

(A) Distribution of pairwise distances between all responsive neurons in S2. Black dashed line shows the average distance between two responsive neurons in S2.

(B) Distribution of pairwise distances between sound-selective and tactile-selective neurons in the same fields of view (blue). Blue dashed line shows the average distance between sound-selective and tactile-selective neurons. Black curve and dashed line reproduced from panel A.

CHAPTER 4

Discussion

In this work, we asked how information from both somatosensory and auditory inputs is integrated in the mouse neocortex. With two-photon Ca^{2+} imaging, we unbiasedly investigated large populations of neurons across somatosensory and auditory areas with single cell resolution. We found that neurons in both S1 and S2 are tuned to different tactile frequencies. The addition of simultaneous sound resulted in modulation of these tactile responses in both S1 and S2, and this modulation typically manifested as a suppression of the response. Moreover, this inhibitory modulation depended on the tactile frequency, with responses to low frequencies more inhibited than responses to high frequencies. We also identified a small but reliable population of neurons (1.2%) in S2 responsive to sound but not to touch. Unlike sound neurons in auditory cortex, sound responses of sound-selective neurons in S2 were strongly inhibited by additional tactile stimuli at high tactile frequencies. These neurons may mediate suppression of nearby touch-selective neurons.

Tactile frequency tuning in somatosensory cortices. The detection of the frequency of mechanical vibrations is important for animals to discern surface texture and to be able to handle tools (Johnson, 2001; Manfredi et al., 2014). Rodents can use the vibration of their whiskers to distinguish smooth surfaces from rough ones (Carvell and Simons, 1990), and neurons in S1 encode information that correlates with texture judgement (von Heimendahl et al., 2007). Thus, it is possible that rodents have neurons in somatosensory cortices tuned to different tactile frequencies, forming a comprehensive representation of surface texture. We found that, while highpass neurons outnumber bandpass neurons in both S1 and S2 (Figures 3D and 3H), the

presence of well-tuned neurons in both regions suggests that tactile frequency tuning might be a general feature for mouse tactile sensation. In addition, the proportion of bandpass neurons was significantly higher in S2 than in S1 ($p < 0.01$). This difference may arise because the two regions receive inputs from different thalamic structures (Bosman et al., 2011). S1 mainly receives thalamic inputs from VPM, while S2 primarily receives thalamic inputs from POm. Interestingly, although both POm and VPM cells show adaptation, causing decreased response amplitude under high frequency stimulation, POm cells exhibit earlier adaptation than VPM cells (Diamond et al., 1992). This difference results in POm cells being tuned to lower frequencies than VPM cells. As S2 neurons receive more inputs from POm than S1, they may, like POm itself, show earlier adaptation to tactile stimuli than S1 neurons. The higher prevalence of bandpass neurons in S2 that we observed (Figure 3) supports this hypothesis.

Sound-driven modulation of tactile responses in somatosensory cortices. We found that the addition of an auditory stimulus modulated tactile responses in both S1 and S2. This modulation has three notable features: 1) Although a similar proportion of neurons in both S1 and S2 were facilitated by sound, more neurons in S2 were inhibited than in S1 (Figure 4F, 5H). 2) Inhibition of bandpass neurons in both S1 and S2 was more severe than inhibition of highpass neurons in the same regions (Figure 4G, 5I). 3) Sound-driven suppression in S1 and S2 are tactile frequency dependent, with stronger inhibition occurring at lower tactile frequencies (Figure 7).

Previous studies in human and primates have revealed that multimodal integration helps with better detection or discrimination of events in the environment (Alais and Burr, 2004; Ernst and Banks, 2002; Fetsch et al., 2009). The optimal integration of competing sensory cues involves dominance of the most reliable sensory cue to minimize variance in the estimation of the true stimulus (Ernst and Banks, 2002). This evaluation of reliability between different sensory cues is

a dynamic process, with the weight or value of each stimulus modality being continuously updated (Fetsch et al., 2009). While we did not determine how sound-driven suppression would help mice better detect their surrounding world in a behavioral context, we note that stimulus salience may be a driving factor behind the multimodal integration observed in our work. In particular, low frequency tactile stimulation is likely more difficult for a mouse to detect and thus less salient of a signal than high frequency tactile stimulation. Consistent with this hypothesis, we observed more suppression of tactile responses at lower tactile stimulus frequencies than at high frequencies (Figure 7), indicating that auditory responses dominate when tactile stimuli are weak. This result is consistent with the prior observation that, during optimal multimodal integration, the more reliable stimulus modality dominates the response. On the other hand, this frequency-dependent integration is complementary to "inverse effectiveness," where multimodal integration is largest for weak multimodal stimuli near threshold and decreases with increasing stimulus intensity, as has been reported in superior colliculus (Perrault et al., 2003; Stanford et al., 2005).

Where does the sound-driven modulation arise? Previously, it was believed that multimodal influence on activity within classically defined unimodal areas is mediated by feedback from multisensory integration in higher-order cortical regions (Foxe and Schroeder, 2005; Macaluso et al., 2000). However, human studies using event-related potentials (ERPs) revealed that this multimodal influence may also be carried in the feedforward inputs coming from subcortical regions to unimodal regions (Foxe and Schroeder, 2005; Giard and Peronnet, 1999; Stein and Stanford, 2008). In the present study, we identified a small (1.2%) but reliable population of sound-selective neurons within S2 itself that may be performing multimodal integration. Although prior studies have shown non-matching neurons, which respond solely to other sensory modality inputs, existing in primary cortices (Wallace et al., 2004), the sound-selective neurons

we found may play a special computational role in multimodal integration. The sound-driven responses in these neurons were strongly suppressed at high tactile frequencies (Figure 8A-E). In contrast, neurons in auditory cortex did not show any suppression by high frequency tactile stimuli (Figure 8F-J). The detection of these rare sound-selective neurons in S2 was aided by the use of two-photon Ca^{2+} imaging, which allowed us to survey hundreds of neurons within a large FOV. We found that sound-selective neurons are only weakly clustered in S2 (Figure 9B), which differs from the strong organization of non-matching neurons seen in other studies (Stein and Stanford, 2008; Wallace et al., 2004). The existence of sound selective neurons in S2 indicates that they may play a role in local sound-driven suppression observed in tactile-selective neurons of S2. Prior work has indicated the presence of direct thalamic inputs from the medial geniculate body to mouse S2, although these projections go to S2 paw regions instead of face regions (Carvell and Simons, 1987). Our finding of sound-responsive neurons in S2 thus suggests the possibility of direct inputs from auditory cortex rather than from auditory thalamus to whisker-responsive regions of S2.

Hypothetical circuit model underlying the sound-driven modulation. Unlike sound-selective neurons of the auditory cortex, auditory responses of sound-selective neurons in S2 are robustly inhibited at high tactile frequencies (>32 Hz). This threshold tactile frequency (32 Hz) matches the inflection point of sound-driven suppression of tactile-selective neurons in S2 (Figure 7). Based on this observation, we hypothesize that local sound-selective neurons in S2 suppress responses of tactile-selective neurons during combined stimulus presentation. In a hypothetical circuit model, tactile-selective neurons (bandpass and highpass neurons) receive tactile inputs, while sound-selective neurons receive auditory inputs. Meanwhile, sound-selective neurons send inhibitory inputs to tactile-selective neurons, while highpass tactile-selective neurons reciprocally

inhibit sound-selective neurons. This winner-take-all circuit can dynamically select the optimal stimulus modality at each moment.

For future studies, circuit manipulation and anatomical tracer studies to verify the functional role of different cell types and their connectivity patterns will be crucial for revealing the mechanisms underlying this phenomenon. Also, behavioral studies will be needed to uncover the ethological significance of tactile-auditory integration and how they are relevant to mice and other animals in the real world.

REFERENCES

Alais, D., and Burr, D. (2004). The ventriloquist effect results from near-optimal bimodal integration. Curr. Biol. CB *14*, 257–262.

Andersen, R.A. (1997). Multimodal integration for the representation of space in the posterior parietal cortex. Philos. Trans. R. Soc. Lond. B. Biol. Sci. *352*, 1421–1428.

Bosman, L.W.J., Houweling, A.R., Owens, C.B., Tanke, N., Shevchouk, O.T., Rahmati, N., Teunissen, W.H.T., Ju, C., Gong, W., Koekkoek, S.K.E., et al. (2011). Anatomical Pathways Involved in Generating and Sensing Rhythmic Whisker Movements. Front. Integr. Neurosci. *5*.

Brosch, M., Selezneva, E., and Scheich, H. (2005). Nonauditory events of a behavioral procedure activate auditory cortex of highly trained monkeys. J. Neurosci. Off. J. Soc. Neurosci. *25*, 6797–6806.

Carvell, G.E., and Simons, D.J. (1987). Thalamic and corticocortical connections of the second somatic sensory area of the mouse. J. Comp. Neurol. *265*, 409–427.

Carvell, G.E., and Simons, D.J. (1990). Biometric analyses of vibrissal tactile discrimination in the rat. J. Neurosci. Off. J. Soc. Neurosci. *10*, 2638–2648.

Chen, T.-W., Wardill, T.J., Sun, Y., Pulver, S.R., Renninger, S.L., Baohan, A., Schreiter, E.R., Kerr, R.A., Orger, M.B., Jayaraman, V., et al. (2013). Ultrasensitive fluorescent proteins for imaging neuronal activity. Nature *499*, 295–300.

Crommett, L.E., Pérez-Bellido, A., and Yau, J.M. (2017). Auditory adaptation improves tactile frequency perception. J. Neurophysiol. *117*, 1352–1362.

Dana, H., Chen, T.-W., Hu, A., Shields, B.C., Guo, C., Looger, L.L., Kim, D.S., and Svoboda, K. (2014). Thy1-GCaMP6 Transgenic Mice for Neuronal Population Imaging In Vivo. PLOS ONE *9*, e108697.

Diamond, M.E., Armstrong-James, M., and Ebner, F.F. (1992). Somatic sensory responses in the rostral sector of the posterior group (POm) and in the ventral posterior medial nucleus (VPM) of the rat thalamus. J. Comp. Neurol. *318*, 462–476.

Diamond, M.E., von Heimendahl, M., Knutsen, P.M., Kleinfeld, D., and Ahissar, E. (2008). "Where" and "what" in the whisker sensorimotor system. Nat. Rev. Neurosci. *9*, 601–612.

Duhamel, J.R., Colby, C.L., and Goldberg, M.E. (1998). Ventral intraparietal area of the macaque: congruent visual and somatic response properties. J. Neurophysiol. *79*, 126–136.

Ernst, M.O., and Banks, M.S. (2002). Humans integrate visual and haptic information in a statistically optimal fashion. Nature *415*, 429–433.

Fetsch, C.R., Turner, A.H., DeAngelis, G.C., and Angelaki, D.E. (2009). Dynamic Reweighting of Visual and Vestibular Cues during Self-Motion Perception. J. Neurosci. *29*, 15601–15612.

Foxe, J.J., and Schroeder, C.E. (2005). The case for feedforward multisensory convergence during early cortical processing. Neuroreport *16*, 419–423.

Foxe, J.J., Wylie, G.R., Martinez, A., Schroeder, C.E., Javitt, D.C., Guilfoyle, D., Ritter, W., and Murray, M.M. (2002). Auditory-somatosensory multisensory processing in auditory association cortex: an fMRI study. J. Neurophysiol. *88*, 540–543.

Frens, M.A., Van Opstal, A.J., and Van der Willigen, R.F. (1995). Spatial and temporal factors determine auditory-visual interactions in human saccadic eye movements. Percept. Psychophys. *57*, 802–816.

Fu, K.-M.G., Johnston, T.A., Shah, A.S., Arnold, L., Smiley, J., Hackett, T.A., Garraghty, P.E., and Schroeder, C.E. (2003). Auditory cortical neurons respond to somatosensory stimulation. J. Neurosci. Off. J. Soc. Neurosci. *23*, 7510–7515.

Giard, M.H., and Peronnet, F. (1999). Auditory-visual integration during multimodal object recognition in humans: a behavioral and electrophysiological study. J. Cogn. Neurosci. *11*, 473–490.

Graziano, M.S., Yap, G.S., and Gross, C.G. (1994). Coding of visual space by premotor neurons. Science *266*, 1054–1057.

Groh, J.M., Trause, A.S., Underhill, A.M., Clark, K.R., and Inati, S. (2001). Eye position influences auditory responses in primate inferior colliculus. Neuron *29*, 509–518.

Haeffele, B., Young, E., and Vidal, R. (2014). Structured low-rank matrix factorization: Optimality, algorithm, and applications to image processing. In Proceedings of the 31st International Conference on Machine Learning (ICML-14), pp. 2007–2015.

von Heimendahl, M., Itskov, P.M., Arabzadeh, E., and Diamond, M.E. (2007). Neuronal activity in rat barrel cortex underlying texture discrimination. PLoS Biol. *5*, e305.

Hikosaka, K., Iwai, E., Saito, H., and Tanaka, K. (1988). Polysensory properties of neurons in the anterior bank of the caudal superior temporal sulcus of the macaque monkey. J. Neurophysiol. *60*, 1615–1637.

Issa, J.B., Haeffele, B.D., Agarwal, A., Bergles, D.E., Young, E.D., and Yue, D.T. (2014). Multiscale optical Ca2+ imaging of tonal organization in mouse auditory cortex. Neuron *83*, 944–959.

Iurilli, G., Ghezzi, D., Olcese, U., Lassi, G., Nazzaro, C., Tonini, R., Tucci, V., Benfenati, F., and Medini, P. (2012). Sound-driven synaptic inhibition in primary visual cortex. Neuron *73*, 814–828.

Jackson, N., and Muthuswamy, J. (2008). Artificial dural sealant that allows multiple penetrations of implantable brain probes. J. Neurosci. Methods *171*, 147–152.

Johnson, K.O. (2001). The roles and functions of cutaneous mechanoreceptors. Curr. Opin. Neurobiol. *11*, 455–461.

Jones, E.G., and Powell, T.P.S. (1970). AN ANATOMICAL STUDY OF CONVERGING SENSORY PATHWAYS WITHIN THE CEREBRAL CORTEX OF THE MONKEY. Brain *93*, 793–820.

Jousmäki, V., and Hari, R. (1998). Parchment-skin illusion: sound-biased touch. Curr. Biol. *8*, R190–R191.

Kanold, P.O., and Young, E.D. (2001). Proprioceptive information from the pinna provides somatosensory input to cat dorsal cochlear nucleus. J. Neurosci. Off. J. Soc. Neurosci. *21*, 7848–7858.

Kayser, C., Petkov, C.I., Augath, M., and Logothetis, N.K. (2005). Integration of touch and sound in auditory cortex. Neuron *48*, 373–384.

Kwon, S.E., Yang, H., Minamisawa, G., and O'Connor, D.H. (2016). Sensory and decision-related activity propagate in a cortical feedback loop during touch perception. Nat. Neurosci. *19*, 1243–1249.

Lederman, S.J., Klatzky, R.L., Morgan, T., and Hamilton, C. (2002). Integrating multimodal information about surface texture via a probe: relative contributions of haptic and touch-produced sound sources. In Proceedings 10th Symposium on Haptic Interfaces for Virtual Environment and Teleoperator Systems. HAPTICS 2002, pp. 97–104.

Lemus, L., Hernández, A., Luna, R., Zainos, A., and Romo, R. (2010). Do sensory cortices process more than one sensory modality during perceptual judgments? Neuron *67*, 335–348.

Lunghi, C., Morrone, M.C., and Alais, D. (2014). Auditory and Tactile Signals Combine to Influence Vision during Binocular Rivalry. J. Neurosci. *34*, 784–792.

Macaluso, E., Frith, C.D., and Driver, J. (2000). Modulation of human visual cortex by crossmodal spatial attention. Science *289*, 1206–1208.

Madisen, L., Garner, A.R., Shimaoka, D., Chuong, A.S., Klapoetke, N.C., Li, L., van der Bourg, A., Niino, Y., Egolf, L., Monetti, C., et al. (2015). Transgenic mice for intersectional targeting of neural sensors and effectors with high specificity and performance. Neuron *85*, 942–958.

Manfredi, L.R., Saal, H.P., Brown, K.J., Zielinski, M.C., Dammann, J.F., Polashock, V.S., and Bensmaia, S.J. (2014). Natural scenes in tactile texture. J. Neurophysiol. *111*, 1792–1802.

McGurk, H., and MacDonald, J. (1976). Hearing lips and seeing voices. Nature *264*, 746–748.

Moran, J., and Desimone, R. (1985). Selective Attention Gates Visual Processing in the Extrastriate Cortex. Science *229*, 782–784.

Olcese, U., Iurilli, G., and Medini, P. (2013). Cellular and synaptic architecture of multisensory integration in the mouse neocortex. Neuron *79*, 579–593.

Peron, S.P., Freeman, J., Iyer, V., Guo, C., and Svoboda, K. (2015). A Cellular Resolution Map of Barrel Cortex Activity during Tactile Behavior. Neuron *86*, 783–799.

Perrault, T.J., Vaughan, J.W., Stein, B.E., and Wallace, M.T. (2003). Neuron-specific response characteristics predict the magnitude of multisensory integration. J. Neurophysiol. *90*, 4022–4026.

Roelfsema, P.R., Lamme, V.A.F., and Spekreijse, H. (1998). Object-based attention in the primary visual cortex of the macaque monkey. Nature *395*, 376–381.

Stanford, T.R., Quessy, S., and Stein, B.E. (2005). Evaluating the operations underlying multisensory integration in the cat superior colliculus. J. Neurosci. Off. J. Soc. Neurosci. *25*, 6499–6508.

Stein, B.E., and Alex, M. (1993). The merging of the senses (Cambridge, MA, US: The MIT Press).

Stein, B.E., and Stanford, T.R. (2008). Multisensory integration: current issues from the perspective of the single neuron. Nat. Rev. Neurosci. *9*, 255–266.

Stein, B.E., Meredith, M.A., Huneycutt, W.S., and McDade, L. (1989). Behavioral Indices of Multisensory Integration: Orientation to Visual Cues is Affected by Auditory Stimuli. J. Cogn. Neurosci. *1*, 12–24.

Treue, S., and Trujillo, J.C.M. (1999). Feature-based attention influences motion processing gain in macaque visual cortex. Nature *399*, 575–579.

Vogelstein, J.T., Packer, A.M., Machado, T.A., Sippy, T., Babadi, B., Yuste, R., and Paninski, L. (2010). Fast nonnegative deconvolution for spike train inference from population calcium imaging. J. Neurophysiol. *104*, 3691–3704.

Wallace, M.T., Meredith, M.A., and Stein, B.E. (1993). Converging influences from visual, auditory, and somatosensory cortices onto output neurons of the superior colliculus. J. Neurophysiol. *69*, 1797–1809.

Wallace, M.T., Ramachandran, R., and Stein, B.E. (2004). A revised view of sensory cortical parcellation. Proc. Natl. Acad. Sci. *101*, 2167–2172.

Wekselblatt, J.B., Flister, E.D., Piscopo, D.M., and Niell, C.M. (2016). Large-scale imaging of cortical dynamics during sensory perception and behavior. J. Neurophysiol. *115*, 2852–2866.

Yau, J.M., Olenczak, J.B., Dammann, J.F., and Bensmaia, S.J. (2009). Temporal frequency channels are linked across audition and touch. Curr. Biol. CB *19*, 561–566.

Yau, J.M., Weber, A.I., and Bensmaia, S.J. (2010). Separate mechanisms for audio-tactile pitch and loudness interactions. Front. Psychol. *1*, 160.

Zhou, Y.-D., and Fuster, J.M. (2004). Somatosensory cell response to an auditory cue in a haptic memory task. Behav. Brain Res. *153*, 573–578.

Zhu, Y., Romero, M.I., Ghosh, P., Ye, Z., Charnay, P., Rushing, E.J., Marth, J.D., and Parada, L.F. (2001). Ablation of NF1 function in neurons induces abnormal development of cerebral cortex and reactive gliosis in the brain. Genes Dev. *15*, 859–876.

Zhuang, J., Ng, L., Williams, D., Valley, M., Li, Y., Garrett, M., and Waters, J. (2017). An extended retinotopic map of mouse cortex. eLife *6*, e18372.

CURRICULUM VITAE

Manning Zhang
mnzhang1013@gmail.com
103 E. Mount Royal Avenue, Apt #501, Baltimore, MD 21202
667-207-3485

EDUCATION

Master of Science in Engineering (expected 05/2017) - Johns Hopkins University, Baltimore, USA
Department of Biomedical Engineering, 09/2015-05/2017

Bachelor of Science in Engineering - Shanghai Jiao Tong University, Shanghai, China
School of Biomedical Engineering, 09/2011-07/2015
School of Medicine, 09/2010-07/2011

Non-degree Coursework Study - National Chiao Tung University, Hsinchu, Taiwan
Department of Electrical and Computer Engineering, Semester-long Exchange Program,02/2013-06/2013

RESEARCH EXPERIENCE

Calcium Signals Laboratory, Johns Hopkins University, **12/2014-Present**
Advisors: David Yue, M.D. Ph.D.; Daniel O' Connor, Ph.D.; John Issa, M.D. Ph.D.; Manu Ben Johny, Ph.D.
- Studied multisensory interactions between tactile stimuli and sound stimuli in mouse somatosensory cortex and auditory cortex.

Theoretical Neuroscience Lab, Johns Hopkins University, **07/2014-09/2014**
Advisor: Kechen Zhang, Ph.D.
- Used Python to analyze multi-electrode EEG data collected from rat hippocampus to uncover temporal patterns of interneuron firing during head-scan behavior involved in the formation of spatial memory.

Electrophysiology and Animal Behavior Lab, Shanghai Jiao Tong University, **02/2012-11/2013**
Advisor: Sheng-tian Li, M.D. Ph.D.
- Evaluated the efficacy of different stimuli (e.g. sleep deprivation, changing electrical field, light flashes of a specific frequency, and auditory stimuli) to induce epileptic seizures of epilepsy in epilepsy mouse models.

PUBLICATIONS

Paper Published in Refereed Journals

Zhou, P., **Zhang, M.**, Zhang, Y., Liu, S., Li, S.-T. (2015) Effects of Mozart K.448 on high-frequency EEG activities in temporal lobe epilepsy model mice. *Journal of Xinyang Normal University*, Nature Science Edition, 2015(02): 177-181.

Conferences

Issa, J.B., Haeffele, B.D., **Zhang, M.**, Young, E.D., Yue, D.T. (2016). "Spatiotemporal response properties across auditory cortical fields under widefield imaging," Assoc. for Res. in Otolaryngology. Abstracts: 507.

Issa, J.B., Haeffele, B.D., **Zhang, M.**, Young, E.D., Yue, D.T. (2015). "Functional architecture of mouse auditory cortex in response to tones and sweeps," Society for Neuroscience Annual Meeting, Chicago, IL.

Presentations

Effects of Music on EEG Activities of Epileptic Model Mice.

Defense of Shanghai Undergraduate Innovation Program (S082IAP005004), 11/2013

Effects of Several Inducible Factors on Epilepsy Seizure and EEG Activities of Epileptic Model Mice.

Defense of Shanghai Jiao Tong University Participation in Research Program (T080PRP21005), 11/2012

ACADEMIC AWARDS

LU YUEJIAO Scholarship for Study Abroad of Shanghai Jiao Tong University, **12/2014**
National Endeavor Fellowship, **12/2013**
Overseas Study Scholarship of Shanghai Jiao Tong university, **11/2012**
Academic Excellence Scholarship of Shanghai Jiao Tong University, **10/2012**

TEACHING EXPERIENCE

Teaching Assistant, System Bioengineering I, Upper-level undergraduate course, Johns Hopkins University, **09/2016 - Present:** Graded student homework assignments.

Teaching Assistant, Systems and Controls, Sophomore-level undergraduate course, Johns Hopkins University, **02/2016-05/2016:** Graded student homework assignments.

Teaching Assistant, System Bioengineering I lab (Cardiovascular regulation stimulation and discussion), Upper-level undergraduate course, Johns Hopkins University, **11/2015:** Helped professor prepare the lab and graded homework and exam.